Thesis for Master's Degree
2020

Estimation of Significant Wave Heights from X-band Radar based on ANN using CNN Rainfall Classifier

Heeyeon Kim

Department of Spatial Design and Engineering
Handong Global University

Thesis for Master's Degree
2020

Estimation of Significant Wave Heights from X-band Radar based on ANN using CNN Rainfall Classifier

Heeyeon Kim

Department of Spatial Design and Engineering
Handong Global University

Estimation of Significant Wave Heights from X-band Radar based on ANN using CNN Rainfall Classifier

Estimation of Significant Wave Heights from X-band Radar based on ANN using CNN Rainfall Classifier

Advisor: Professor Kyungmo Ahn

By

Heeyeon Kim

Department of Spatial Design and Engineering

Handong Global University

A thesis submitted to faculty of the Handong Global University in partial fulfillment of the requirements for the degree of Master of Engineering in the Department of Spatial Design and Engineering

December 28, 2020
Approved by

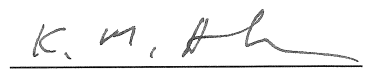

Professor Kyungmo Ahn
Thesis Advisor

Estimation of Significant Wave Heights from X-band Radar based on ANN using CNN Rainfall Classifier

Heeyeon Kim

Accepted in partial fulfillment of the requirements for the degree of Master of Engineering

December 28, 2020

Thesis Advisor

Prof. Kyungmo Ahn

Committee Member

Prof. Sangmo Jeong

Committee Member

Prof. Cheo K. Lee

SD&E Kim Heeyeon
21933002
Estimation of Significant Wave Heights from X-band Radar based on ANN using CNN Rainfall Classifier
Graduate School of Spatial Design and Engineering
, 2020. 58p.

Advisor: Prof. Kyungmo Ahn.

ABSTRACT

The coast is a space that is easy for humans to access and use in various ways. However, since the understanding of physical phenomena occurring on the coast is not complete, continuous observation and research on the coast have been conducted. Although the X-band radar, one of the remote sensing equipment, is less accurate, it is easy to maintain and has no restrictions on water depth, therefore many studies have been conducted to improve the performance.

As artificial neural network (ANN) models that generate functions from non-linear data have recently improved, it is introduced to the field of coastal observation. Several studies proved that ANN-based X-band radar system for significant wave heights (Hs) estimation shows high performance. However, the quality of the radar image is significantly degraded during rainfall causing low accuracy in Hs estimation. Therefore, in this study, improved ANN model is proposed to increase the accuracy of estimation of Hs during rainfall or typhoon accompanied by heavy rain.

To automatically classify radar images into rainy and non-rainy cases, a convolutional neural network (CNN), which is known to exhibit excellent performance in image classification, is used. Then, an algorithm for calculating Hs is proposed by creating two different ANN models and selectively applying them according to the rainfall. As a result, the coefficient of determination of the estimated Hs and the reference Hs (measured by Coastal Wave-rider Buoy (CWB)), slightly increased from 0.81 to 0.85. The high waves underestimated during typhoons are reasonably corrected.

TABLE OF CONTENTS

ABSTRACT ..... **i**
TABLE OF CONTENTS ..... **iii**
LIST OF FIGURES ..... **iv**
LIST OF TABLES ..... **vi**

1. INTRODUCTION **1**
1.1 Research background and Motivation 1
1.2 Literature reviews 2
1.3 Research Objective and Thesis Organization 4
2. THEORETICAL STUDY AND RESEARCH DATA **7**
2.1 Wave spectrum analysis of radar images 7
2.2 CNN(Convolutional Neural Network) 10
2.3 ANN(Artificial Neural Network) 16
2.4 Research data 18
3. RAINFALL CLASSIFICATION USING CNN **23**
3.1 Data process 23
3.2 CNN rainfall classifier 27
3.3 Result 28
4. IMPROVED Hs ESTIMATION ALGORITHM BASED ON ANN **31**
4.1 Parameters for ANN 31
4.2 Hs estimation algorithm and ANN models 38
4.3 Results and discussion 44
5. CONCLUSION **46**
6. REFERENCES **48**
APPENDIX **51**
A. Summary of Hs estimation during the typhoon Maysak(2020/09/03) 51
B. Summary of Hs estimation during the typhoon Haishen(2020/09/07) 55

LIST OF FIGURES

Figure 1. Examples of X-band radar images of clear-windy case (left) and rain-contaminated case (right) 2
Figure 2. (a) Time series of Hs from radar (red) and buoy (black), (b) Time series of errors of radar (black) and rainfall intensity (blue) 5
Figure 3. Overview of spectrum analysis of radar image 7
Figure 4. The reflection condition by Bragg resonance of radar signal 9
Figure 5. General structure of convolutional neural network 11
Figure 6. Convolution process between image and weight filter 12
Figure 7. ReLU function 13
Figure 8. Sub-extration process 14
Figure 9. Classification process 15
Figure 10. Algorithm overview of Artificial Neural Network 16
Figure 11. Principle of Neural Network 17
Figure 12. Location of X-band radar, AWS and Buoy and observation range of X-band radar 18
Figure 13. Overview of 3-S System 19
Figure 14. X-band radar installed on the roof of the Maple Beach Hotel located on the Anin cast in Gangneung 20
Figure 15. AWS at Gangmun 22
Figure 16. Procedure of CNN rainfall classification 23
Figure 17. Cropped radar images as input data for CNN 24
Figure 18. Examples of radar images classified based on rainfall data. (a) rain case, (b) no-rain case. 25
Figure 19. Model structure of CNN rainfall classifier 27
Figure 20. Result of CNN rainfall classification 30
Figure 21. Time series of buoy Hs 32
Figure 22. Time series of buoy Hs for typhoon season in 2020 32

Figure 23. Time series of X-band radar parameters for whole period. (a) Signal, (b) Noise, (c) $\sqrt{SNR}$ 34
Figure 24. Time series of X-band radar parameters for typhoon season in 2020. (a) Signal, (b) Noise, (c) $\sqrt{SNR}$ 36
Figure 25. Regressions of parameters with Hs buoy. (a) signal, (b) noise, (c) $\sqrt{SNR}$ ... 37
Figure 26. Overview of proposed algorithm 38
Figure 27. Input variables of ANN1 40
Figure 28. Input variables of ANN2 41
Figure 29. Regressions of estimated Hs and Hs buoy. (a) rain data, (b) no-rain data. 42
Figure 30. Flow of model application of a single data 43
Figure 31. Regression of results (a) single ANN (b) multiple ANN(the proposed algorithm) 45

LIST OF TABLES

Table 1. Specification of X-band radar system 20
Table 2. Model training information of CNN for rainfall classification 28
Table 3. Result summary of CNN rainfall classification..... 29
Table 4. Model training information of ANN1 and ANN2 for Hs estimation..... 39

1. INTRODUCTION

1.1 Research background and Motivation

The coast is widely used as a space for economic and cultural activities. Real-time wave observation is essential to prevent human accidents and property damage and ensure safe entry and exit of ships, safe leisure activities, and coastal structures' stability.

Widely used methods for coastal wave observation include direct observation and remote observation. Direct observation is measuring the water surface's displacement using pressure gauge, wave-rider buoy or ADCP(Acoustic Doppler Current Profiler). Remote observation method is using remote sensor such as a radar. Although the direct observation method has high accuracy, there is a limit to the depth of installation since it is installed on the sea surface or the seafloor. It is difficult to maintain because it is exposed to extreme ocean environment. Besides, the data is collected at only one point where the device is installed.

On the other hand, remote sensing device such as radar is installed on land or structures. Therefore, the maintenance is easy because they are not affected by the marine environment. It is possible to obtain two-dimensional information on the sea by scanning a large area. This study attempted to develop a highly accurate wave observation system using marine X-band radar. X-band radar is a sensor usually installed on ships and used for navigation.

The standard method for estimating the significant wave heights (Hs) is using the correlation between the SNR and Hs. SNR, signal to noise ratio, is calculated from the radar image through image spectrum analysis. However, once the quality of the radar image is degraded due to severe weather such as heavy rainfall and typhoons, the quality of the SNR gets also degraded. Then the estimated Hs is unstable. As shown in Figure 1, raindrops

randomly appear on the radar images and noise increases significantly during rainfall. Hence, the accuracy of the X-band radar for estimation of Hs decreases.

Recently, for estimating Hs, an artificial neural network (ANN) method using various wave information other than SNR has been studied. ANN reflects the nonlinearity between the radar image and Hs. However, Hs errors still occur when rainfall noise occurs on the radar images. Therefore, it is required to develop an improved or a new Hs estimation algorithm that reflects the characteristics of radar images during severe rains or typhoons.

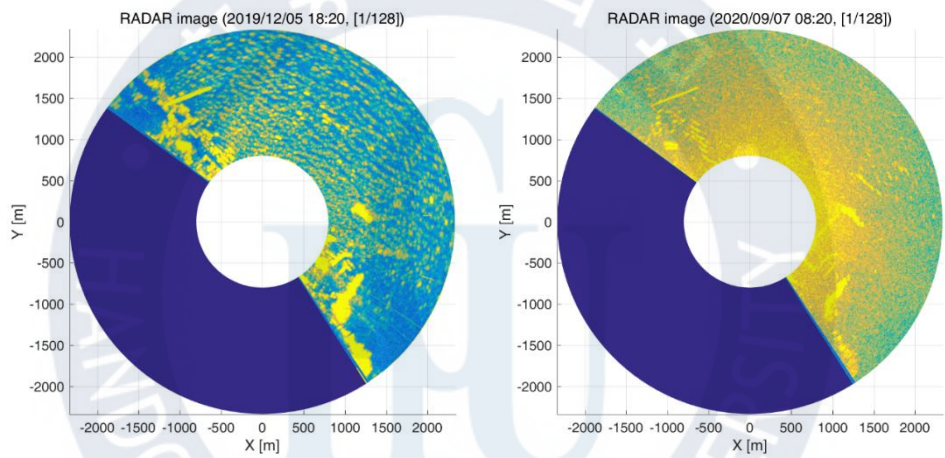

Figure 1. Examples of X-band radar images of clear-windy case (left) and rain-contaminated case (right)

1.2 Literature reviews

The primary method widely known for Hs estimation using X-band radar is to use the SNR calculated from the radar image spectrum through 3D fast Fourier transform (FFT). Alpers and Hasselmann (1982) suggested that the $\sqrt{SNR}$ and the Hs of SAR (Synthetic Aperture Radar) images have a linear relationship. Nieto et al. (2004) and Nieto et al. (2008) also used an FFT-based spectrum analysis method. They applied dispersion equations and

employed modulation transfer functions (MTF) to the X-band radar image spectrum. Also, they systematically organized X-band radar-based wave analysis techniques. Ahn et al. (2014) showed improved Hs estimation by using a simple nonlinear relationship between Tp (peak period) and Hs. However, the correlation between $\sqrt{SNR}$ and Hs varies depending on the weather conditions. In real world, the accuracy of the Hs calculated using the linear relationship with $\sqrt{SNR}$ is very low.

Recently, several studies have been conducted to estimate the Hs by applying an ANN to reflect the nonlinearity caused by weather dependence. Vicen et al. (2012) tried a multilayer perceptron-based Hs estimation method using wavelength and wave period as input variables. Park et al. (2017) proposed a single-layer ANN model using SNR, wave period, and radar quality factors as input variables. These studies for estimating Hs using ANN showed significantly improved results. Nevertheless, when the quality of the radar image is bad in environments such as rain or typhoon accompanied by heavy rain, then there is still a problem that a large error occurs in the estimated Hs.

On the other hand, a wave observation study is attempted using EMD (Empirical Mode Decomposition) analysis, not FFT, led Huang and Liu. Liu et al. (2016a) conducted a comprehensive wave analysis using EMD with X-band radar images, but they excluded rain-contaminated radar images. In the same year, Liu et al. (2016b) estimated the wind direction using EMD from rain-contaminated X-band radar images. The study implied the possibility of estimating Hs through EMD in rain-noisy radar images. Meanwhile, various studies on the quality improvement and quality control of remote observation data such as HF radar (High Frequency Radar), MWR (MIROS Wave and Current Radar), and X-band radar have been continuously conducted (Gomez et al., 2014; Gurgel et al., 2011; Hisaki,

2009; Jun et al., 2020).

CNN for image recognition was firstly introduced by LeCun et al. (1989). Since then, CNN algorithms have been generalized by Behnke (2003) and Simard et al. (2003), GP-GPUs have spread and mass computing technology has developed, CNN have been used in many fields requiring image recognition. Hakim (2020) attempted to classify rainfall from CCTV images using CNN and showed 98.3% accuracy.

1.3 Research Objective and Thesis Organization

The purpose of this study is to improve the accuracy of estimation of Hs based on ANN during rainfall and typhoons. This study proposes an improved algorithm corrected from the ANN model studied at the Institute of Construction and Environment of Handong Global University. The existing algorithm estimates the Hs using a single ANN model without considering rainfall. However, in the improved algorithm, the final Hs is calculated by selecting an appropriate ANN model for Hs estimation according to the rainfall.

Figure 2 compares the estimation of Hs with the buoy Hs data during the period of typhoon Maysak and Haishen occurred in September 2020. Figure 2 (a) shows the time series of estimated Hs (red) with the Hs of buoy (black). This estimation is performed using a single ANN algorithm of the model and variables proposed by Park et al. (2017). Figure 2 (b) shows the difference between the Hs measured by radar and Hs measured by wave-rider buoy (black). The hourly rainfall observed at the Gangmun Automatic Weather System (AWS) post in Gangneung is plotted together (blue).

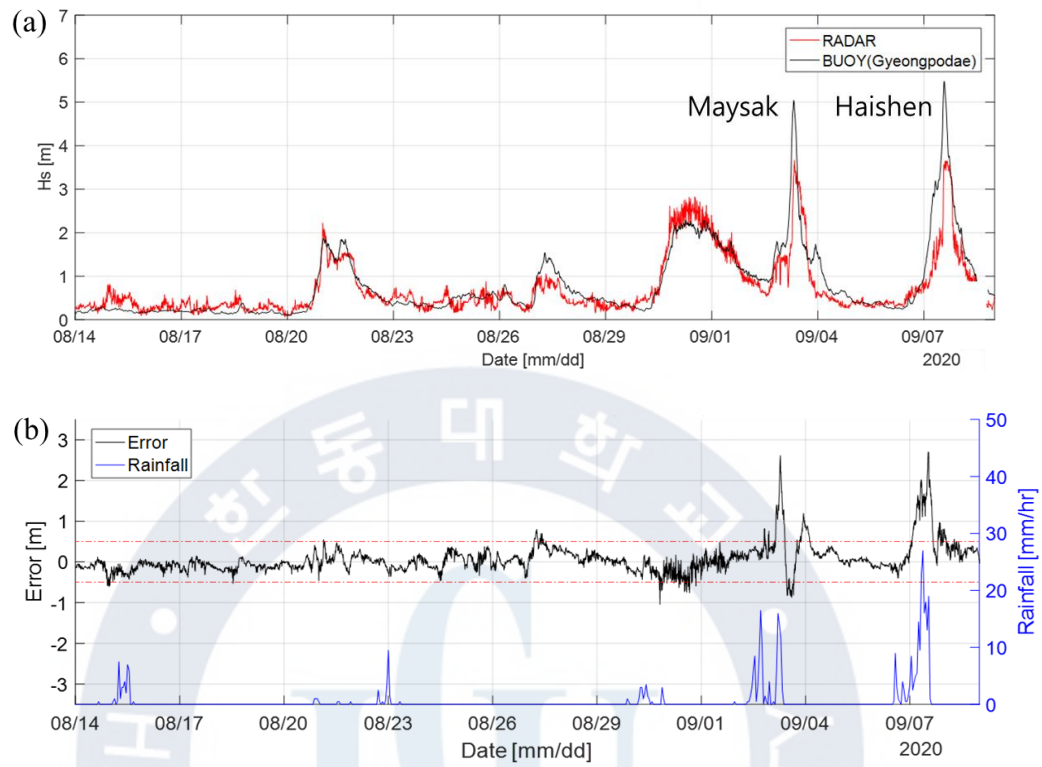

Figure 2. (a) Time series of Hs from radar (red) and buoy (black), (b) Time series of errors of radar (black) and rainfall intensity (blue)

It seems that errors of Hs from the X-band radar increase during typhoon, and rainfall accompanied during the period. This study is aimed at improving the accuracy of Hs estimation during the typhoon Maysak and Haishen which hit the Korean Peninsula in September, 2020. Full analysis data are radar images from January 2019 to September 2020. First, we developed a CNN model that automatically classifies radar images according to rainfall. Second, ANN models for Hs estimation are developed using the classified radar image.

The structure of this paper is as follows. Chapter 2 explains the principle of obtaining various wave parameters from X-band radar images and the theory of CNN and ANN. Chapter 3 describes the process of classifying rainfall from radar images using CNN. Chapter 4 describes the proposed ANN algorithm to estimate Hs. Finally, in Chapter 5, Conclusions are presented.

2. THEORETICAL STUDY AND RESEARCH DATA

2.1 Wave spectrum analysis of radar images

Wave observation using X-band radar is possible by analyzing images generated by backscattered electromagnetic waves at sea surface. The radar image is time-series (t) data of two-dimensional (x, y) coordinates. In other words, radar image is spatial and temporal data which represents the signals reflected from the sea surface. The radar image, expressed as $\eta(x, y, t)$, is transformed into a spectrum in the frequency and wavenumber domain through three-dimensional fast Fourier transform (3D FFT). Figure 3 shows the process of analyzing the radar image and extracting variables used to estimate the Hs. The results of spectrum analysis include parameters such as Signal, Noise, SNR, Tp (peak period), and Wave direction. Signal is the sum of energy of wave components extracted from radar image. Noise is the sum of energy of non-wave component. SNR means signal to noise ratio.

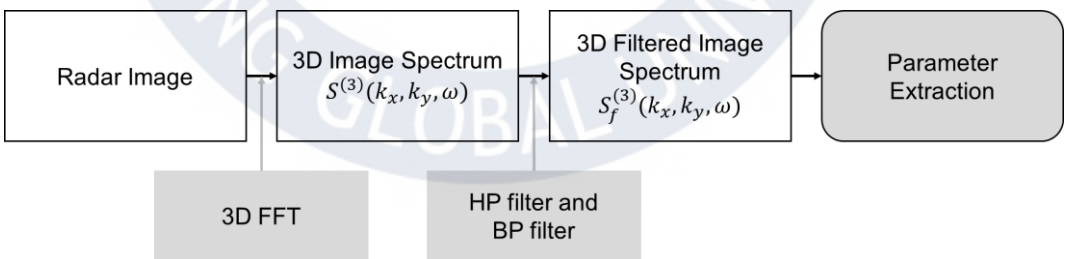

Figure 3. Overview of spectrum analysis of radar image

Radar image data is discrete data. Since the power density function $S(k_x, k_y, \omega)$ obtained using DFT always has a leakage error, a window function is used to reduce the

leakage error. In this study, the *hann* function provided by MATLAB is used in the process of FFT.

On the other hand, stagnant structures and background noise are included in the energy spectrum. They are usually concentrated in the low frequency band. To remove the noises in the low-frequency band, high-pass filter is applied to the energy spectrum. The high-pass filtered spectrum is $S_{HP}(k_x, k_y, \omega)$. The wave components which satisfy the dispersion equation are filtered by applying band-pass filter to the spectrum. From the band-passed wave spectrum $S_{BP}(k_x, k_y, \omega)$, variables such as Signal, Noise, and SNR are calculated as following Equations 1 to 3. Signal is calculated by integrating the wave spectrum. Since the Noise is the sum of non-wave components, it is calculated by subtracting Signal from the total energy. SNR represents the ratio of signal and noise.

$$(Signal) = \iiint S_{bp}(\mathrm{k}_x, \mathrm{k}_y, \omega)\,\mathrm{dk}_x\, dk_y d\omega \tag{1}$$

$$(Noise) = \iiint S_{hp}(\mathrm{k}_x, \mathrm{k}_y, \omega)\,\mathrm{dk}_x\, dk_y d\omega - (Signal) \tag{2}$$

$$SNR = \frac{(Signal)}{(Noise)} \tag{3}$$

Meanwhile, the three-dimensional spectrum is integrated for the frequency or two-dimensional wavenumber to obtain a wavenumber spectrum and a frequency spectrum, respectively. By integrating these, the Peak period (Tp) and Wave direction (Pdir) are calculated. The formulas are as follows:

$$Tp = \frac{2\pi}{\omega_p}, \quad S_{BP}(k_x, k_y, \omega_p) = \max(S_{BP}(k_x, k_y, \omega)) \tag{4}$$

$$Pdir = \tan^{-1}\left(\frac{k_{yp}}{k_{xp}}\right), \quad S_{BP}(k_{xp}, k_{yp}, \omega) = \max(S_{BP}(k_x, k_y, \omega)) \tag{5}$$

Since the parameters are derived through the image spectrum analysis, radar-based observation of waves highly depends on the quality of the radar image. The condition for obtaining a high-quality radar image is that the Bragg resonance occurs and the intensity of the backscattered signal is amplified. Bragg resonance is a phenomenon in which radio waves are amplified when the wavelength of ripple is close to the half wavelength of a radar electromagnetic wave due to blowing wind. The relationship between the two wavelengths is as follows:

$$\lambda_s = \frac{\lambda_r}{2\sin\theta} \tag{6}$$

where λ_r is electromagnetic wavelength and λ_r is ripple wavelength.

Figure 4 shows the reflection condition by Bragg resonance of radar signal.

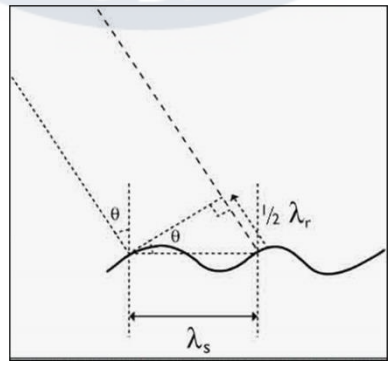

Figure 4. The reflection condition by Bragg resonance of radar signal

By Bragg resonance, wave parameters are calculated through spectrum analysis. In general, when the wind is not blowing well, the intensity of radar wave signal tends to be low because the intensity of the received radar signal is weak. Then the accuracy of estimated Hs gets lower at the same time.

The standard method for estimating Hs using X-band radar uses the relationship between the Hs and SNR proposed by Alpers and Hasselmann (1982) as follows:

$$H_s = A + B\sqrt{SNR} \tag{7}$$

However, this relationship is oversimplified because there are many environment variables in the real world. Equation 7 is occasionally not suitable for use in the field except when radar shows distinct images in windy days. Therefore, in order to consider the cases of bad backscattering signals, the ANN-based Hs estimation method is introduced. The variables obtained through wave spectrum analysis and other data related to wind are used as input parameters in ANN models.

2.2 CNN(Convolutional Neural Network)

Machine learning works like a black box that automatically creates functions based on input and output data. Machine learning exhibits excellent performance in nonlinear problems where it is challenging to define functional expressions, though it is not easy to interpret the physical characteristics of the trained model.

Machine learning includes supervised and unsupervised learning. Supervised learning is a learning method when the input data and the corresponding output data are known. Supervised learning includes linear models, decision trees, support vector machines

(SVMs), and neural networks (NN). On the other hand, unsupervised learning generates relations only using input data without given corresponding output data, for example, algorithms such as clustering.

Convolutional Neural Network (CNN) is one of supervised learning. This deep learning technology summarizes and extracts features of an image and classifies it into a group value. The training process of CNN model includes input, feature extraction, and classification, as shown in Figure 5.

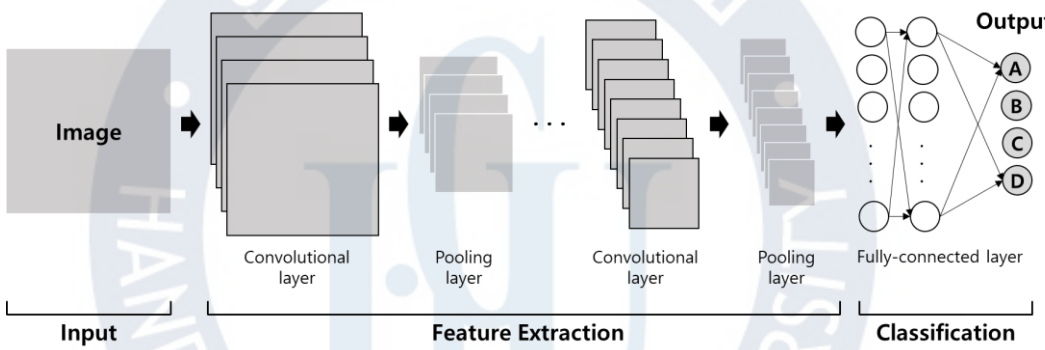

Figure 5. General structure of convolutional neural network

Once an image entered, the features of the image are extracted through the convolution layer. The convolution operation is repeated between the convolution weight filter and the image. When multiple convolution filters are used on an image having complex features, more diverse features can be extracted from the image. Strictly, it is not a convolution but a cross-correlation operation because it does not reverse the function to be operated. The formula for the actual cross-correlation operation is as follows:

$$(f * g)(i, j) = \sum_{x=0}^{h} \sum_{y=0}^{w} f(x, y) g(i + x, j + y) \tag{8}$$

For the convenience, the cross-correlation operation is called as a convolution in this study.

The equation of the feature extracted by the convolution operation is as follows:

$$y_{\tilde{i}\tilde{j}} = \sum_{i}^{h} \sum_{j}^{w} W_{ij} \times x_{\tilde{i}+i, \tilde{j}+j} + b \tag{9}$$

where the input image is x and the extracted feature map is y. W is the weight filter for convolution. i and j are the position of the weight value in the filter, and w and h are the size of the filter. b is the bias of the convolutional filter. Learning a CNN model means finding optimal weights and biases through iterative calculations. Figure 6 simply shows the convolution process of an image. A convolution filter with a size smaller than that of the image moves over the image and adds the result of multiplying the overlapping components to create a feature map.

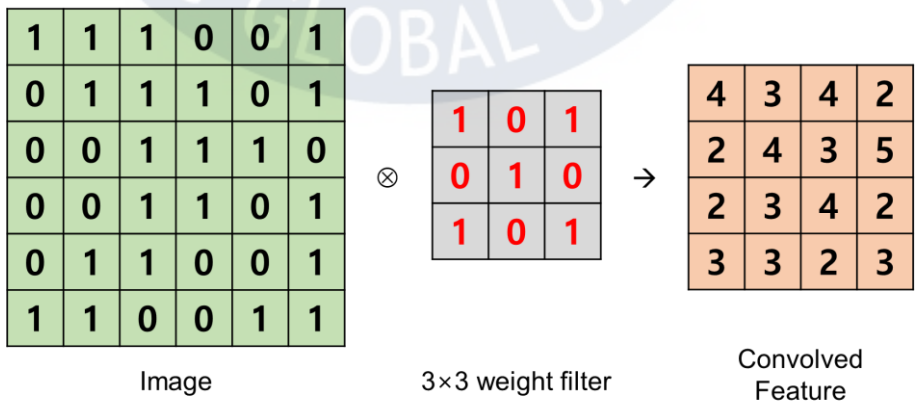

Figure 6. Convolution process between image and weight filter

By applying the activation function to the result of the convolution operation, a feature map is created. ReLU (Rectified Linear Unit) function is used as the activation function. The ReLU function ignores negative values in the feature map and transfers only positive information to the next process. The ReLU function is expressed as shown in Figure 7.

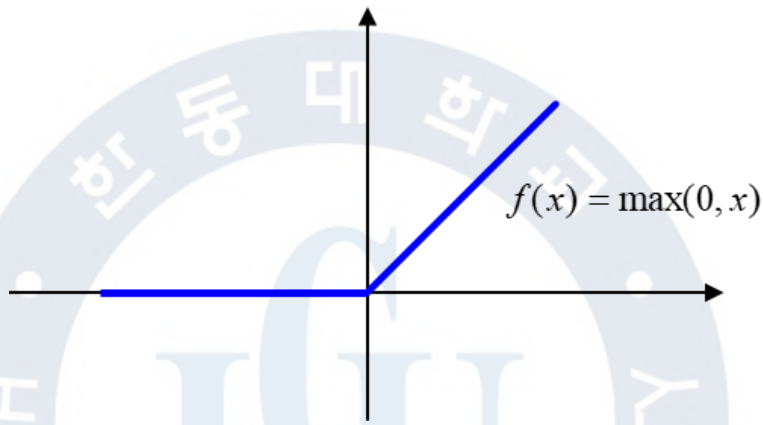

Figure 7. ReLU function

Compared to the sigmoid function and hyperbolic tangent function, the ReLU function has the advantage of simple operation and much faster learning. However, since the slope is 0 for the data of x<0, there is a disadvantage that neurons may be lost.

Extracted feature map is reduced through a sub-sampling process. It is to remove unnecessary information and degree of noise. The sub-extraction include max-pooling and average-pooling method. In this study, feature maps are reconstructed using maximum-value extraction techniques. The sub-extraction process is shown in Figure 8.

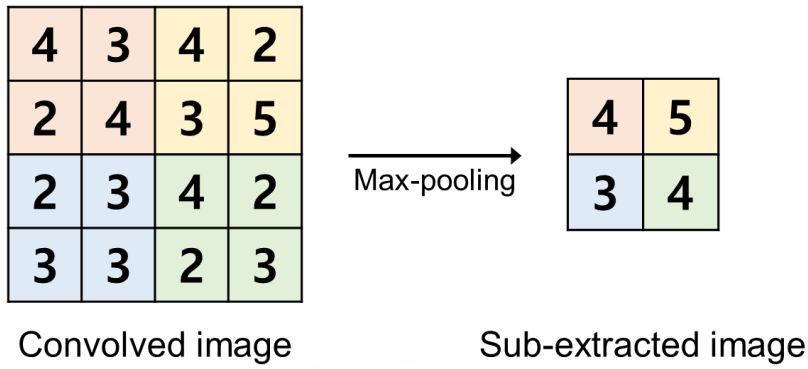

Figure 8. Sub-extration process

After repeating the convolutional layer and the sub-extraction layer alternatively for several times, they are rearranged as a one-dimensional vector like in a general ANN structure in the classification step. The output is obtained using a fully-connected layer connected to several neural network nodes. The probability values of each result category are obtained by applying the log-softmax function to the output value. The category with the largest probability value is the classification result of the image. Figure 9 shows how to get the final classification result using the fully connected layer and the activation function.

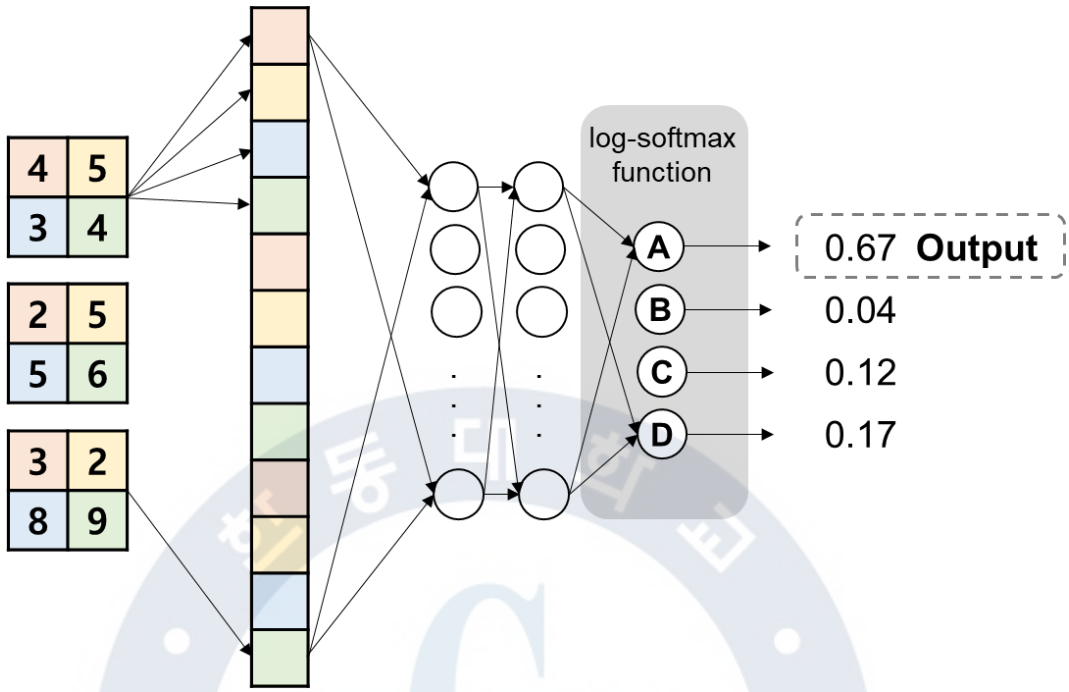

Figure 9. Classification process

A general ANN converts input data into a one-dimensional vector from the beginning, whereas a CNN can learn associations with surrounding pixels of an image. Therefore, it shows high classification accuracy even when the target object has rotation, deformation, or size changes.

Meanwhile, the data for supervised learning of a neural network consists of a training dataset, a verification dataset, and a test dataset. Training dataset is for model training, verification dataset is for accuracy evaluation, and the test dataset is for application of the model. In general, 80 to 90% of the data is used for model training, and the remaining 10 to 20% of the data is used to verify the accuracy of the model.

Cross-validation is performed to correctly evaluate the model's accuracy. Cross-validation is performed by learning 3 to 5 models while changing the combination of

trainset so that the training data and verification data do not overlap and calculate the average accuracy.

2.3 ANN(Artificial Neural Network)

Artificial neural network (ANN), one of supervised learning, is machine learning algorithm created by imitating human neurons. Most of the data obtained from nature are difficult to grasp a linear relationship or a generalized relationship. ANN is a powerful algorithm that connect multiple artificial neurons to learn complexity and nonlinearity of data. The algorithm overview of ANN is shown in Figure 10.

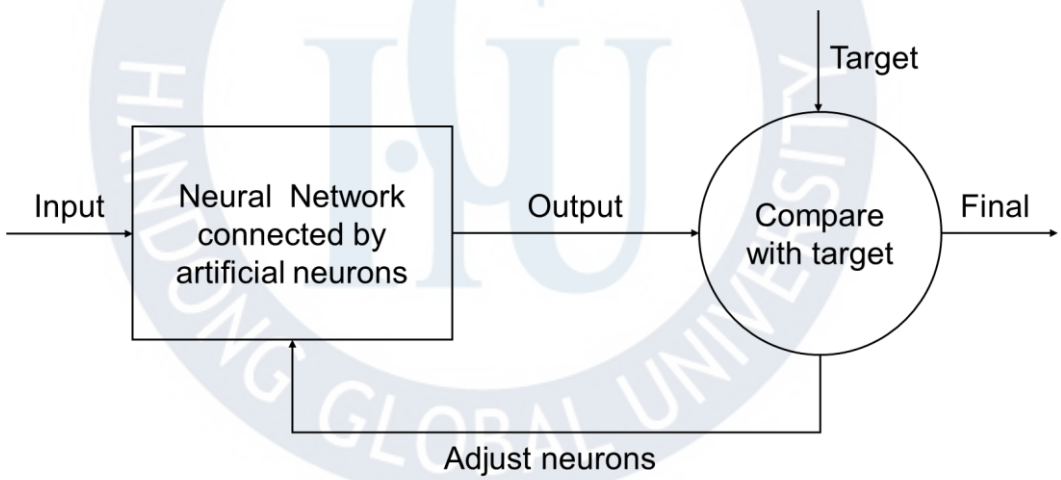

Figure 10. Algorithm overview of Artificial Neural Network

ANN creates optimal neurons by repeatedly comparing the results of applying weights and biases with target data at the artificial neurons (or artificial nodes). This neuron mimics human nerve cells. The principle of operation of the ANN is expressed as shown in Figure 11.

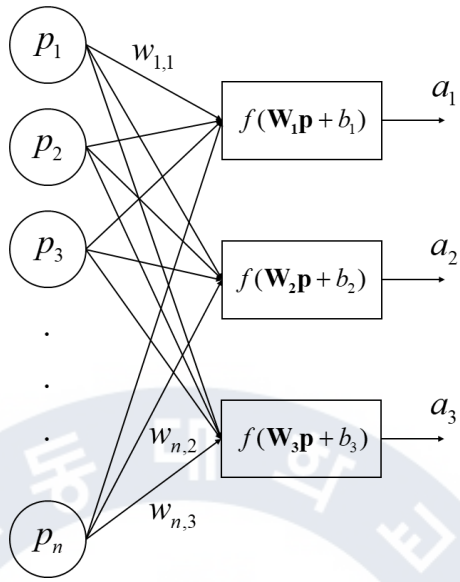

Figure 11. Principle of Neural Network

A simple formula that expresses the process occurring in individual neurons of the ANN is as follows:

$$a = f(wp + b) \tag{10}$$

where w is the weight and b is bias. f is the transfer function, and a is the result value of a node. Each node multiplies the input data by the weight, adds the bias, and then outputs the result (a) using the transfer function (f). The result calculated by the node is transferred to the next node. If the error of estimated result with the target value in the final layer is less than a certain level, the iteration is terminated and the final result comes out. Through repeated comparison and learning with the target value, each node of the ANN finds the optimal weight and bias value. In this way, one artificial neural network model is trained.

2.4 Research data

The data used in the study are the X-band radar images, Hs of the Coastal Wave Buoy (CWB) at Gyeongpodae Beach, and rainfall data from the Gangmun Automatic Weather System (AWS). The locations where the data is collected are shown in Figure 12.

Figure 12. Location of X-band radar, AWS and Buoy and observation range of X-band radar

2.4.1 X-band radar images

X-band radar uses a frequency of about 8 to 12 GHz and is a device commonly used for ship navigation, object detection, and weather observation. In the X-band radar image, sea

clutter backscattered from the sea surface appears on a 2D plane in a radius of about 2 km from where the radar is installed. Since the radar periodically observes sea surface, radar images are given as time series data. Various wave information such as Signal, Noise, SNR, and Peak period(Tp) can be obtained by spectral analysis of this radar image of sea clutter (Alpers and Hasselmann 1982; Nieto et al., 2004).

In this study, X-band radar is installed on the roof of the Maple Beach Hotel located on the Anin coast in Gangneung. The picture of the X-band radar is as shown in Figure 14. The radar system used in this study is 3-S System, developed by Gopher and Instruction of Construction and Environment Research of Handong Global University. The radar system includes X-band radar, software, hardware, and wind gage. Wind data is additionally used to train ANN model for Hs estimation. The wind gage measures wind direction and wind speed. Figure 13 shows the overview of 3-S System.

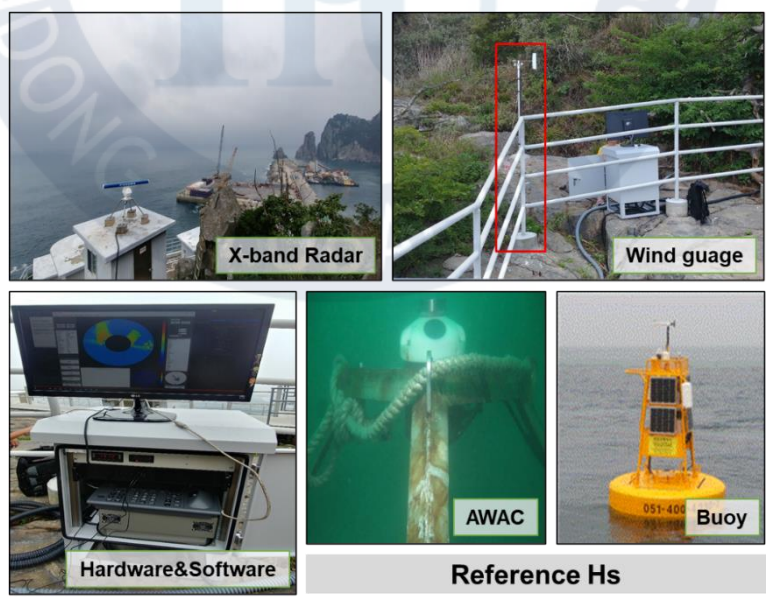

Figure 13. Overview of 3-S System

A horizontally polarized radar using X-band electromagnetic waves of about 9.4 GHz is used. Data is obtained by observing a radius of about 8km to 2.3 km at an altitude of about 30m. The location of the radar system and the observation range are shown in Fig 12. 79,843 X-band radar images are collected from November 2018 to September 2020. One set of observation is 3 minutes long and it consists of 128 radar images. Radar observation before 2019/06/30 was performed every 20 minutes, and thereafter was performed every 10 minutes. Table 1 shows the temporal and spatial resolutions of the X-band radar system installed at the Anin Beach in Gangneung.

Table 1. Specification of X-band radar system

RPM	Δt	Δr	$\Delta\theta$	Maximum range	Time length of observation	Installation height
42	1.42sec	1.5	0.3°	2.33km	183 or 366sec	30m

Figure 14. X-band radar installed on the roof of the Maple Beach Hotel located on the Anin cast in Gangneung

2.4.2 Wave-rider buoy data at Gyeongpodae

Meteorological Administration provides Hs data of Coastal Wave Buoy (CWB) at the position of Gyeongpodae Beach. Hs obtained from the wave-rider buoy is used to train the ANN models for Hs estimation and to verify the accuracy. The installation location of the buoy at Gyeongpodae Beach is shown in Figure 12, and the appearance of the buoy equipment is shown in Figure 14. For the ANN-based Hs estimation, reference data (or target data) is necessary. It is best to collect the reference data by installing direct observation devices such as ADCP(Acoustic Doppler Current profiler) or CWB ("buoy" for short) at the same position as shown in Figure 13. However, since Gyeongpodae Beach is about 8km away from the X-band radar location, it is somewhat inaccurate to directly compare with the Hs calculated from the radar image. This data is inevitably used due to the limitations of data collection. Hs of CWB is provided almost in real-time, every 5 minutes. Hs modified for outliers is provided on 15th of the following month.

2.4.3 Gangmun AWS Rainfall data

To train the CNN model for the classification of rainfall and verify the accuracy, Gangmun AWS rainfall data used as a label. AWS provides rainfall data in units of minute, hour, day, month, and year. 1-minute rainfall data is used in this study. Rainfall data also has limit of not accurately reflecting the rainfall situation at the radar installation point. The distance from Gangmun AWS and the X-band radar is about 6.7 km. However, this limit is supplemented by manually excluding abnormal data when collecting CNN model training data. Gangmun AWS location and AWS equipment are shown in Figure 12 and Figure 15, respectively.

Figure 15. AWS at Gangmun

3. RAINFALL CLASSIFICATION USING CNN

This chapter explains the process of classifying whether the X-band radar image is an image during rain or a non-rainfall time using CNN. First, preprocessing radar images and rainfall data for CNN training is described. Second, the model configuration of the CNN classifier is described in order. Finally, we discuss the results and accuracy of rainfall classification results of radar images. Figure 16 shows the procedure of rainfall classification. Later, the classified result is sent to ANN algorithm for Hs estimation.

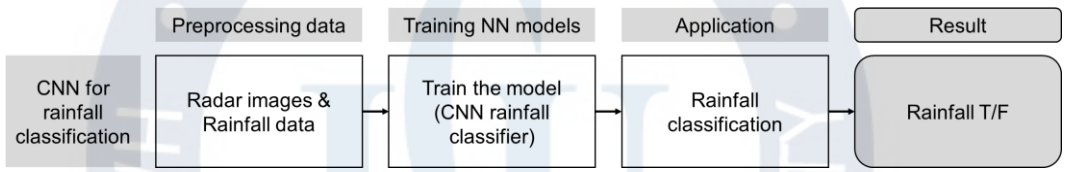

Figure 16. Procedure of CNN rainfall classification

3.1 Data process

3.1.1 Crop radar images

In CNN for image classification, since the input data is a 2D image, the computation time and computation cost vary widely depending on the size of the image. The input data of CNN to classify rainfall is a high-resolution image of the size 512×1080 (512 in radial direction and 1,080 in azimuth) observed with an X-band radar. However, it is unnecessary to use the entire radar image to determine rainfall from the image. Therefore, to reduce unnecessary computation time, a part of the radar image was cut out and used as input data for CNN, as shown in Figure 17. The cropped image is a square of 200×200 size which

corresponds to a $600m \times 600m$ sea-surface area. It sufficiently includes waves and rainfall noises. The selected area is out of obstacles and the structures of the sea.

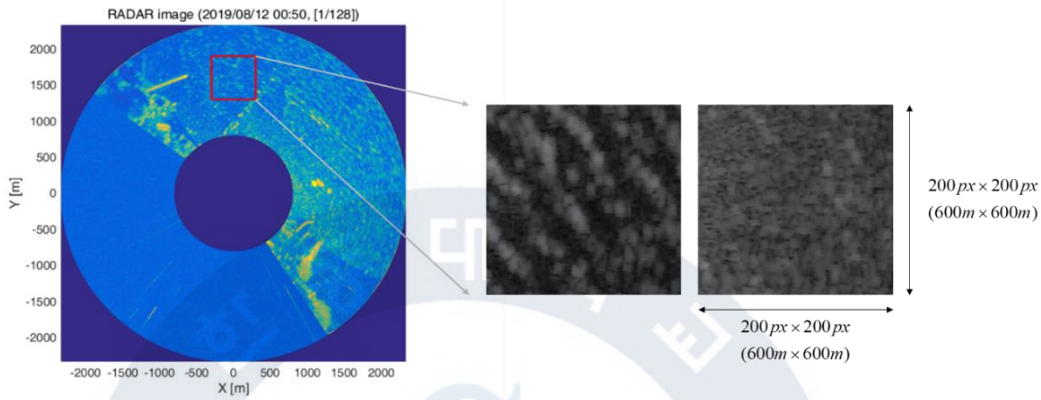

Figure 17. Cropped radar images as input data for CNN

3.1.2 Preprocess rainfall data

The label value indicating rainfall in the radar image was used by correcting the 1-minute rainfall data provided by Gangmun AWS. Since one radar image is about 3 minutes long, the 1-minute rainfall data from the Gangmun Station is moving averaged over 3 minutes and converted into binary data indicating rainfall. If the value is positive, it is written as 1, and if the value is negative, it is written as 0.

3.1.3 Select radar images for model training

For the CNN model to exhibit high performance in classification, it is essential to construct the training dataset elaborately. The classification performance of the model can be trusted only by learning with data that clearly shows the features between groups to be classified. However, in this study, there is a problem that the rainfall value and precipitation

appeared in the radar image do not exactly match because the Gangmun AWS is slightly away from the radar point. To compensate for this limit, the training dataset was manually adjusted.

First, the cropped radar images are labeled based on the rainfall label. An example of a labeled radar image is shown in Figure 18.

Figure 18. Examples of radar images classified based on rainfall data. (a) rain case, (b) no-rain case.

Figure 18 (a) is a radar image classified as when it rains and (b) when it does not rain. When it rains, the radar image tends to have a large pixel value due to rainfall noise, and the image that appears to have no rainfall noise is included. This is the case that rainfall

noise does not occur even though it is raining (outlier) or the case of non-rainfall data included (mis-classified). On the other hand, in the classified as non-rainfall in Figure 18 (b), there is a tendency that the overall pixel value is low. It is because wave sometimes appears or nothing appears. However, it is confirmed that an excessive wave (outlier) is indistinguishable from rainfall noise with the naked eye or that there are rainfall data mis-classified.

Second, the outliers and mis-classified data shown above are excluded from the training dataset according to a simple formula. If the average value of the pixel brightness among the images during rainfall is significantly low, or the average value of the brightness values among the images during non-rainfall times is significantly larger, it is excluded from the training data. As an exclusion criterion, $[\mu-\sigma, \mu+\sigma]$, which is a range containing about 68% of the data in the distribution of the average pixel brightness value, is used. μ_i denotes the average pixel brightness value of individual radar images, and σ denotes the standard deviation of the average pixel brightness value distribution of all radar image data. When the radar image i is an image, during rainfall and the average pixel brightness value I_i is less than $\mu-\sigma$, the images is excluded from the training data set. When the radar image i is an image, during rain and the average pixel brightness value I_i is greater than $\mu+\sigma$, the radar images are excluded from the training dataset.

The training dataset was rearranged in the above way. And, the abnormal data are additionally removed while observing with the naked eye.

3.2 CNN rainfall classifier

3.2.1 Model structure

The CNN model for the rainfall classification is configured by repeating the convolutional layer twice and generating the classification result through the fully connected layer. The structure of the CNN model and the size of each layer are listed in Figure 19.

Input layer 200 × 200 (1)
Convolution layer 5 × 5 (10)
max-pooling 2 × 2
Convolution layer 5 × 5 (20)
max-pooling 2 × 2
Fully-connected layer (50)
Fully-connected layer (2)
Log-softmax function
Output

Figure 19. Model structure of CNN rainfall classifier

The input data is a radar image of a size of 200×200, and there is one channel. In the first convolution layer, a 5×5 convolution weight filter is used, and the number of channels is expanded to 10. In the second convolutional layer, a 5×5 filter is used in the same way, and the channels are expanded to 20. For both cases, the data size is reduced by maximum pooling method with a window of 2×2. In the classification step, the results of the convolutional layer are sequentially connected to two fully-connected layers consisting of 50 nodes and 2 nodes. Finally, a high probability value among the two result groups of

rainfall and non-rainfall is taken and extracted as a classification result using the log-softmax function.

3.2.2 Model training

Table 2 shows the overview of model training information of CNN rainfall classifier. As training data, 7,783 radar images from 2019/07/01 to 2019/10/03 are used, in which 3,422 are rainfall samples and 4,361 are non-rainfall samples.

Table 2. Model training information of CNN for rainfall classification

Train Set	Data period	2019.07.01. ~ 2019.10.03.
	Data ratio	Total 7,783 Rain sample 3,422(44%) No-rain sample 4,361(56%)
Test Set	Data period	2018.11.23. ~ 2020.09.20.
Label data		Gangmun AWS 1-minute rainfall data 2018.11.23. ~ 2020.9.20.

3.3 Result

In general, 80-90% of the data is used for learning(training), and 10-20% are used for testing and verification to evaluate the accuracy of the model. In this study, however, since the final purpose is estimation of Hs, the accuracy of CNN rainfall classifier is not strictly verified by distinguishing the verification data. Instead, the accuracy is evaluated based on the result of applying the entire analysis data to the model.

Table 3 shows the summary of result and the accuracy of classifying rainfall for 79,843 X-band radar images collected from 2018/11/23 to 2020/09/20 at Gangneung Anin Beach. When it rains, it is expressed as P (positive), and when it does not rain, it is expressed as N (Negative). Therefore, the rainfall classification result is classified into TP (true positive), FP (false positive), FN (false negative), and TN (true negative). Accuracy is the sum of TP and TN divided by the total number of analyzed data. 8% of the total analysis data corresponds to learning data. In general, considering that the accuracy of the CNN image classifier with a simple structure is over 90%, the classification accuracy of radar image rainfall is 93.9%, which is evaluated as having relatively good classification performance. Of the 6.1% of classification errors, 5.7% of the cases are false positives classified as raining when it did not rain. This is because the wind blows well and the dense wave appearing on the radar image looks like rain noise.

Table 3. Result summary of CNN rainfall classification

	Number of data	Percentage(%)
True Positive(TP)	13,002	16.3
False Positive(FP)	4,519	5.7
False Negative(FN)	316	0.4
True Negative(TN)	62,006	77.7
Total Polulation	79,843	100
Accuracy	$\frac{TP+TN}{Total\ Population}=\frac{75,008}{79,843}$	93.9

Figure 20 partially shows the results of CNN rainfall classification, which is rain or no-rain. Result before October 3, 2019 is trained part and model simulated part is after that. Blue bars show the true rainfall and red dots mean CNN result.

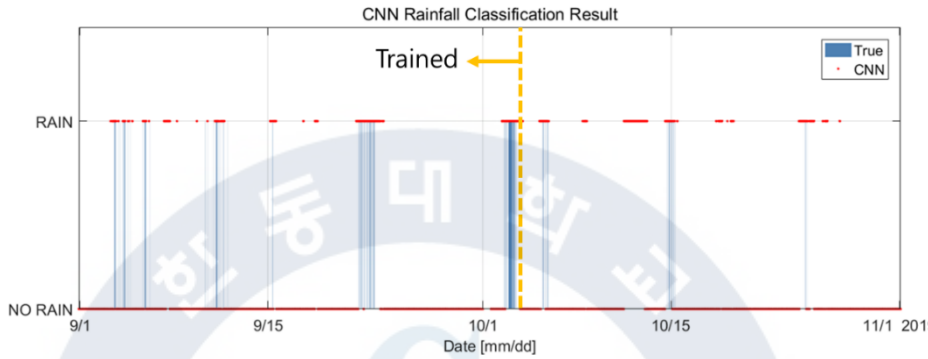

Figure 20. Result of CNN rainfall classification

4. IMPROVED Hs ESTIMATION ALGORITHM BASED ON ANN

This chapter describes the algorithm for calculating the Hs using ANN. The ANN model used in this study is a model referring to the models proposed by Vicen et al. (2012) and Park et al. (2017). Existing studies on ANN-based Hs estimation using X-band radar images have used a single ANN model. In this study, however, an algorithm using multiple ANN model is proposed which is designed to cover the case of bad weather such as heavy rainfall or typhoon not only the usual cases.

The proposed algorithm is that, for each temporal data, an ANN model is automatically selected among several pre-trained models according to the data's rainfall label, and the final Hs is calculated by simulating the chosen model for given data. 4.1 observes feature of parameters, the input parameters and the target parameter. The reason for applying different ANN models according to rainfall can be found in the variable observation stage. 4.2 describes the overall algorithm and ANN models for estimation of Hs. The idea of the algorithm for selecting an ANN model according to rainfall can be found in model application stage. In 4.3, Hs estimation results are presented and discussed.

4.1 Parameters for ANN

4.1.1 Target parameter

Buoy Hs measured at Gyeongpodae CWB(Coastal Wave Buoy) point is the target parameter to train ANN models for Hs estimation. It means that the buoy Hs is considered

as reference value. CWB Hs is provided every 5 minutes almost in real-time. The Hs data modified with outliers is provided on 15th of the following month. In this study, the real-time Hs is brought and data-processing is performed in the laboratory by removing outliers and calculating moving averages. The time series of Hs measured by buoy from January 1, 2019 to September 20, 2020 is shown in Figure 21.

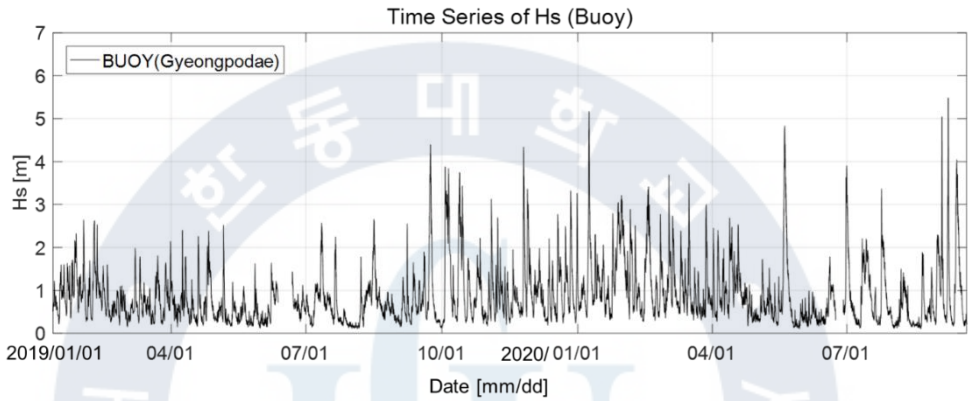

Figure 21. Time series of buoy Hs

Also, the time series of Hs of buoy in the period of typhoons is shown in Figure 22. The peak Hs during the typhoon Maysak is 5.05m and that of Haishen is 5.48m.

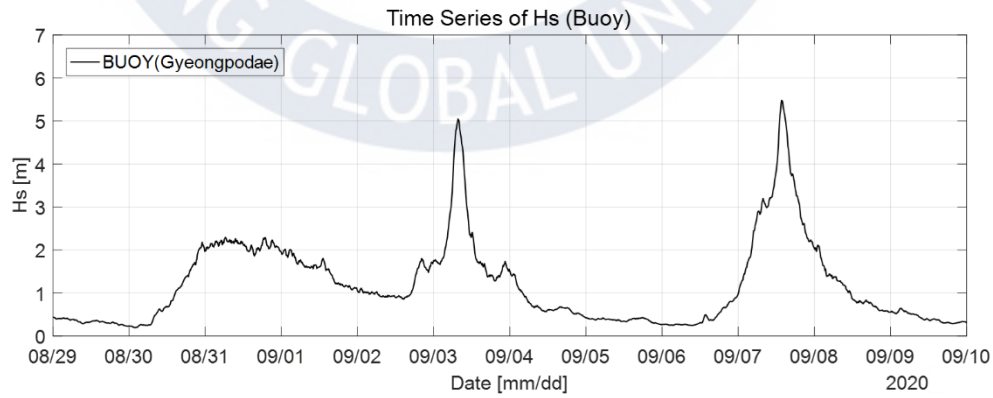

Figure 22. Time series of buoy Hs for typhoon season in 2020

4.2.2 Input parameters

The input variables used for training the ANN model in this paper are signal, noise, $\sqrt{SNR}$, peak period, wind direction, and maximum wind speed. $\sqrt{SNR}$, signal, noise, and Tp is calculated by radar image spectrum analysis. Wind direction and maximum wind speed is measured from wind gage of 3-S System. According to Alpers and Hasselmann(1981), since the $\sqrt{SNR}$ calculated through radar image analysis has a linear relationship with the significant wave height, Signal, Noise, and $\sqrt{SNR}$ are regarded as the most representative variables in the ANN-based Hs model. Figure 23 shows the time series of Signal(a), Noise(b), and $\sqrt{SNR}$ (c) from January 1, 2019 to September 20, 2020.

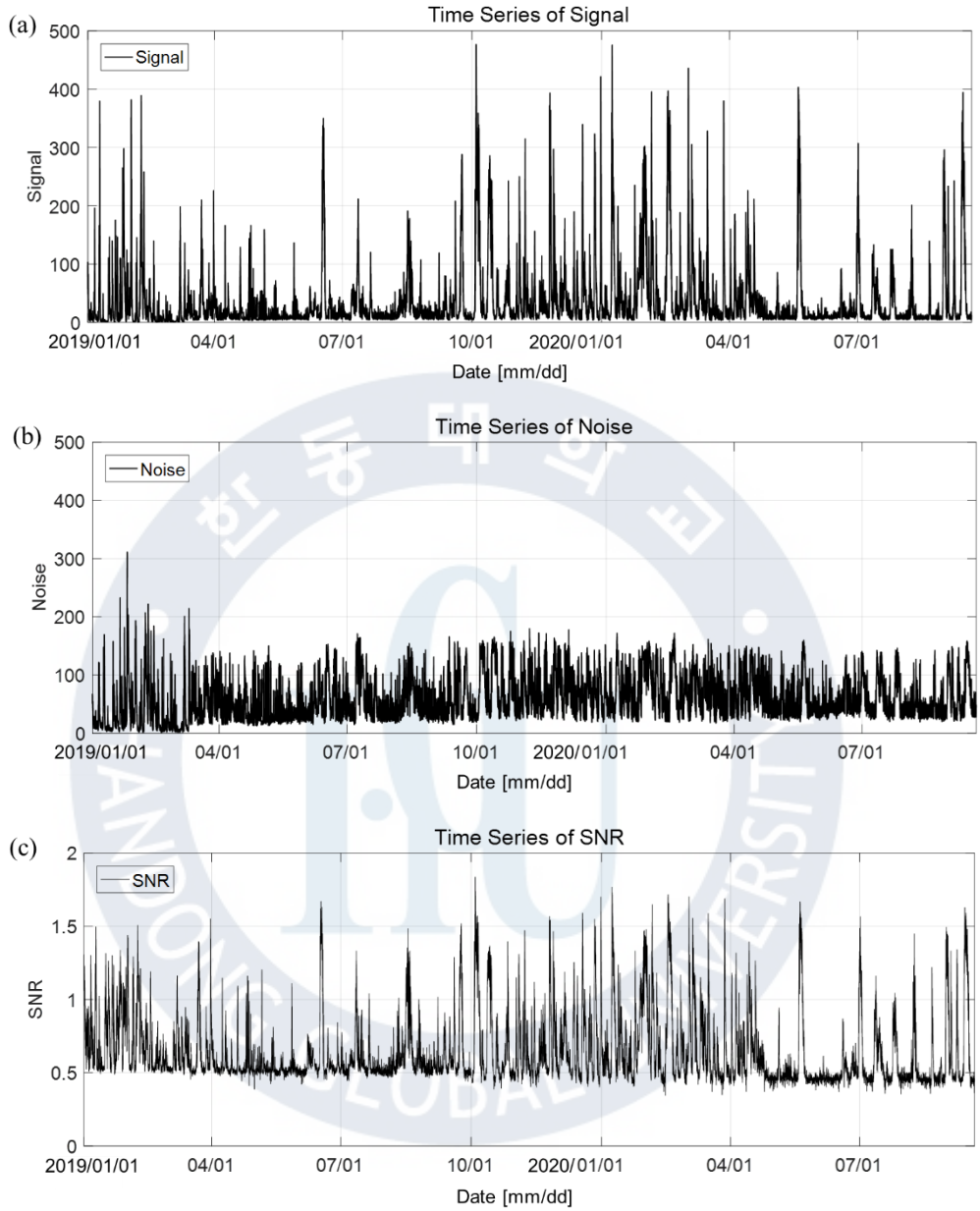

Figure 23. Time series of X-band radar parameters for whole period. (a) Signal, (b) Noise, (c) $\sqrt{SNR}$.

Figure 24 shows the time series of signal(a), noise(b), and $\sqrt{SNR}$ (c) for the period of typhoons Maysak and Haishen hit the Korean Peninsula in 2020. Peaks are found on September 3 for Maysak and on September 7 for Haishen. It is expected that there was a storm from around August 30th to around September 2nd. It was confirmed that it did not rain during this period.

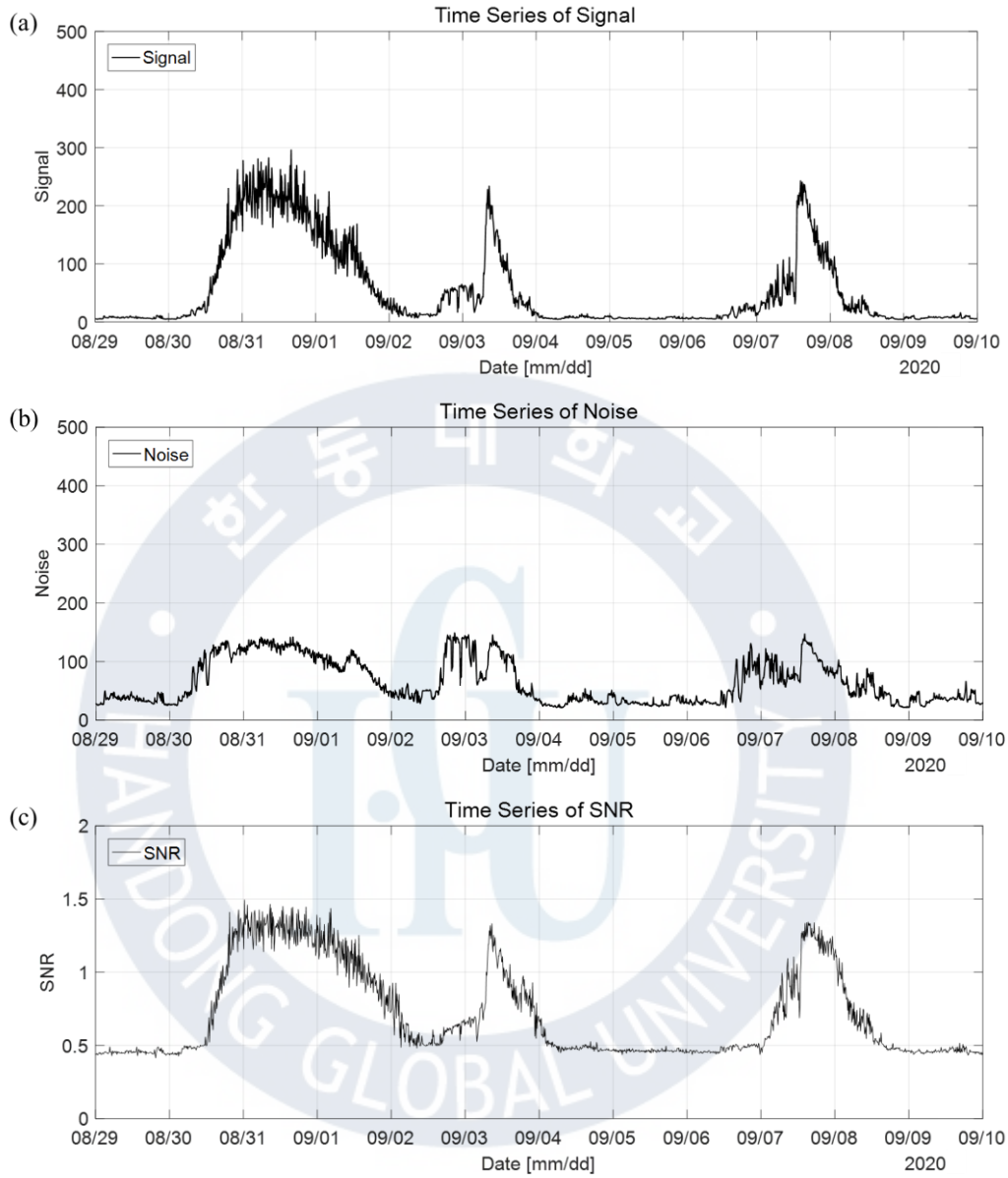

Figure 24. Time series of X-band radar parameters for typhoon season in 2020. (a) Signal, (b) Noise, (c) $\sqrt{SNR}$.

Figure 25 shows simple regression of signal(a), noise(b), and $\sqrt{SNR}$ (c) with Hs measured by buoy. Rainfall and non-rainfall data is expressed in blue and black,

respectively. In Figure 25 (a), Red line shows the simple regression line between Signal and Hs, and it is found that rainfall data and non-rainfal data have different regression relationships with Hs. Especially for Noise, in Figure 25 (b), rainfall data show no clear relationship with Hs. The main reason is that random noises appear on radar images when it rains. Inevitably rainfall and non-rainfall data of $\sqrt{SNR}$ also have different regression relationships with Hs as shown in Figure 25 (c).

Therefore, for reliable Hs estimation, it is rational thought that different ANN models should be used depending on rainfall. In the chapter 4.2, how to apply different ANN models according to rainfall is described in detail.

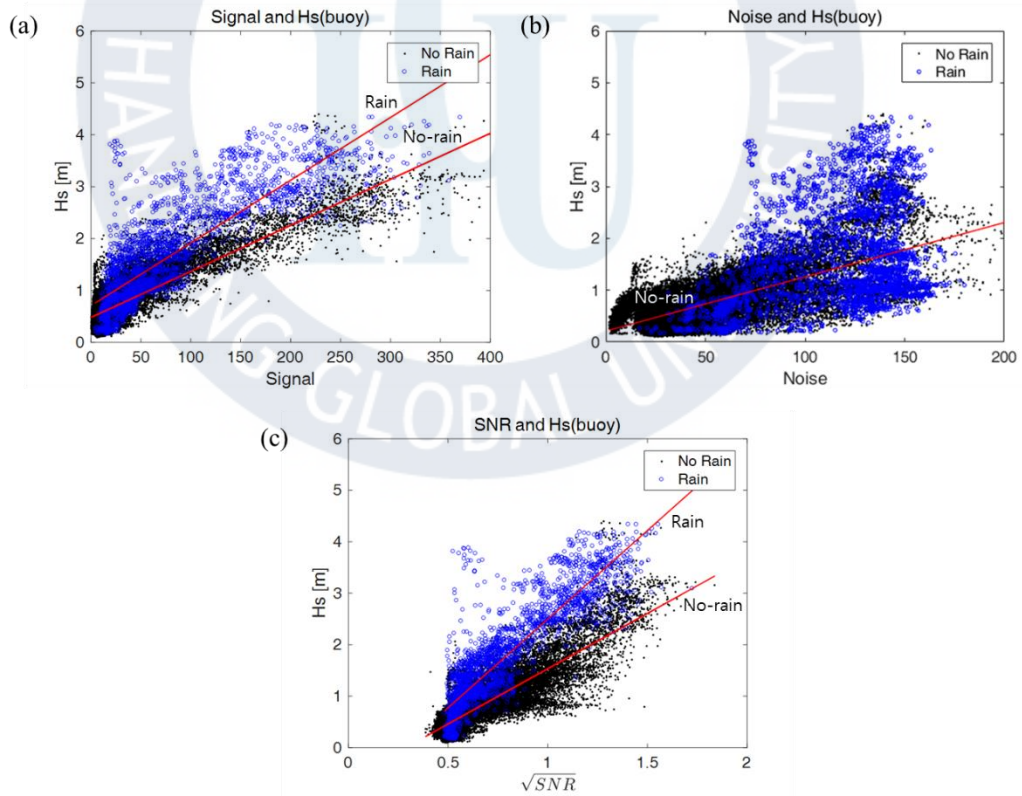

Figure 25. Regressions of parameters with Hs buoy. (a) signal, (b) noise, (c) $\sqrt{SNR}$

4.2 Hs estimation algorithm and ANN models

4.2.1 Algorithm of Hs estimation based on ANN

Figure 26 shows the overview of proposed algorithm of Hs estimation. First, preprocess the input variables and reference data (or target data) to train ANN models. The prepared input variables are Signal, Noise, $\sqrt{SNR}$, Tp (peak period), Wind direction and Wind speed. The reference data is Hs measure by buoy. Second, train several models changing combinations of input variables or sampling methods. Two models are trained for Hs estimation in this study. Third, bring the time series of rainfall T/F label and select an ANN model according the label. Lastly, apply the selected model to the data and get the final Hs.

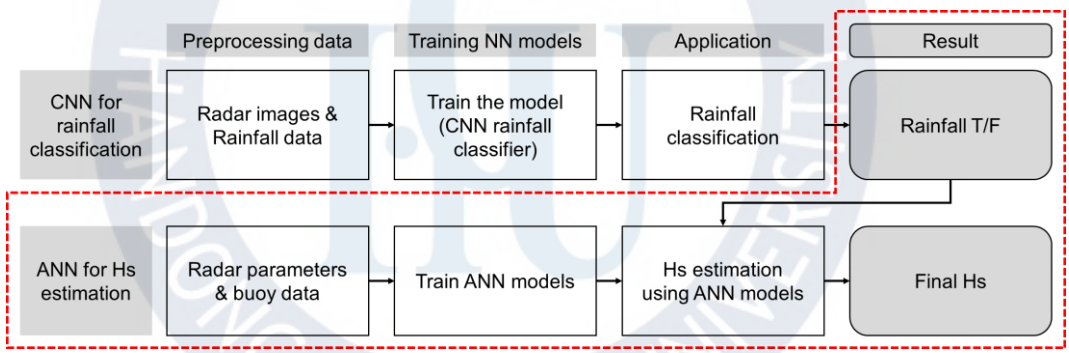

Figure 26. Overview of proposed algorithm

4.2.2 ANN models for Hs estimation

In this study, two ANN models are trained, ANN1 and ANN2, to cover bad weather conditions. Information on model training is described in Table 4. The data period of Hs estimation is from 2019/01/01 to 2020/09/20. The reference Hs is buoy Hs data from Gyeongpodae Buoy point. Train data is sampled in a period of from 2019/01/01 to 2020/07/31 for both ANN1 and ANN2 regardless of rainfall. The trained model was applied

to the data from 2020/08/01 to 2020/09/20, and Hs at the time of typhoons Maysak and Haishen invaded in September was examined.

Table 4. Model training information of ANN1 and ANN2 for Hs estimation

ANN1	Train data	Equal interval sampling within 2019.01.01. ~ 2020.07.31.
	Input parameters	Signal, Noise, SNR, Tp, Pdir, Ws, and Max/Min value of each parameter for past 6 hours
ANN2	Train data	Local Max/Min sampling within 2019.01.01. ~ 2020.07.31.
	Input parameters	Signal, SNR, Tp, Ws, and Max/Min value of Ws for past 6 hours
Reference Hs		Gyeongpodae Buoy Hs 2019.01.01. ~ 2020.09.20.
Simulation data		2020.08.01. ~ 2020.09.20.

ANN1 is general model which shows good estimation in normal case. 6 types of input variables are used to train the model ANN1 as shown in Figure 27, those are SNR, Signal, Nosie, Tp, Wind direction, and Maximum 10-minute wind speed. Also, the minimum and the maximum value of each parameter for past 6 hours is used as input data. Therefore, the number of input parameters is 18. Training data is sampled by selecting data at equal

interval, that is, every 3.5 days.

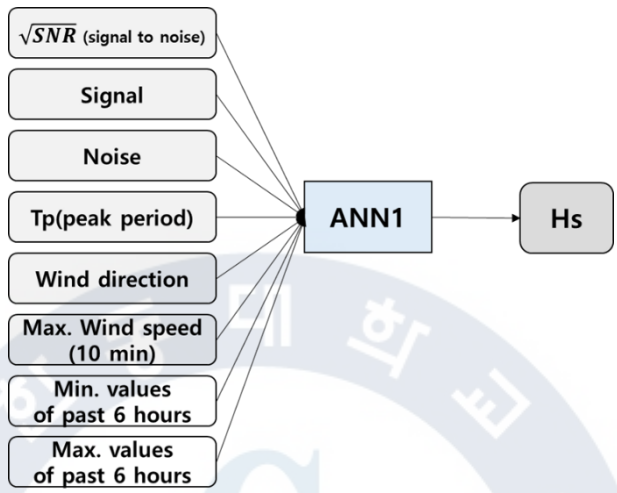

Figure 27. Input variables of ANN1

ANN2 is a model which shows good estimation when it rains or there is a typhoon. Noise and Wind direction is excluded from the configuration of input parameters of ANN1. The reason of removal of Noise and Wind direction is that the Noise is less correlated with Hs during rainfall, and the Wind direction fluctuates heavily in all direction. Minimum and maximum values of each parameters are also removed from the input parameter table but including those of Wind speed. Wind speed is an important parameter in bad weather condition. Therefore, the proportion of the wind speed variable has increased. The input parameters are 4 types, that is, $\sqrt{SNR}$, Signal, Tp, and Wind speed as shown in Figure 28. The number of input variables of ANN2 is 6 including Min/Max Wind speed for past 6 hours.

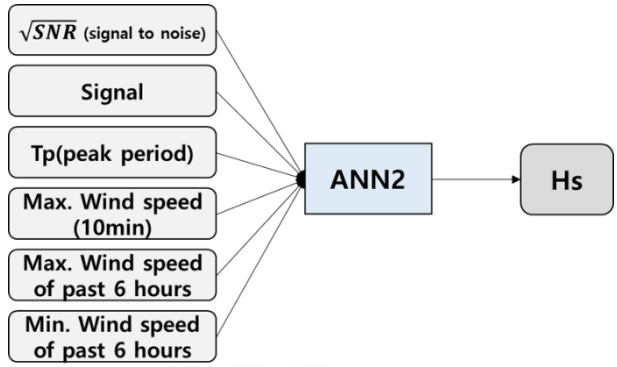

Figure 28. Input variables of ANN2

Figure 29 shows the regressions of the estimated Hs and the reference buoy Hs. The black data is the result of applying the model ANN1 and the red data is of ANN2. All data is applied to ANN1 and ANN2, and they are plotted separately along rainfall. In Figure 29 (a), it is found that high waves of rain data over than 3m tend to be underestimated when applied ANN1. Contrary, low waves of non-rainfall data are overestimated when applied ANN2 in Figure 29 (b).

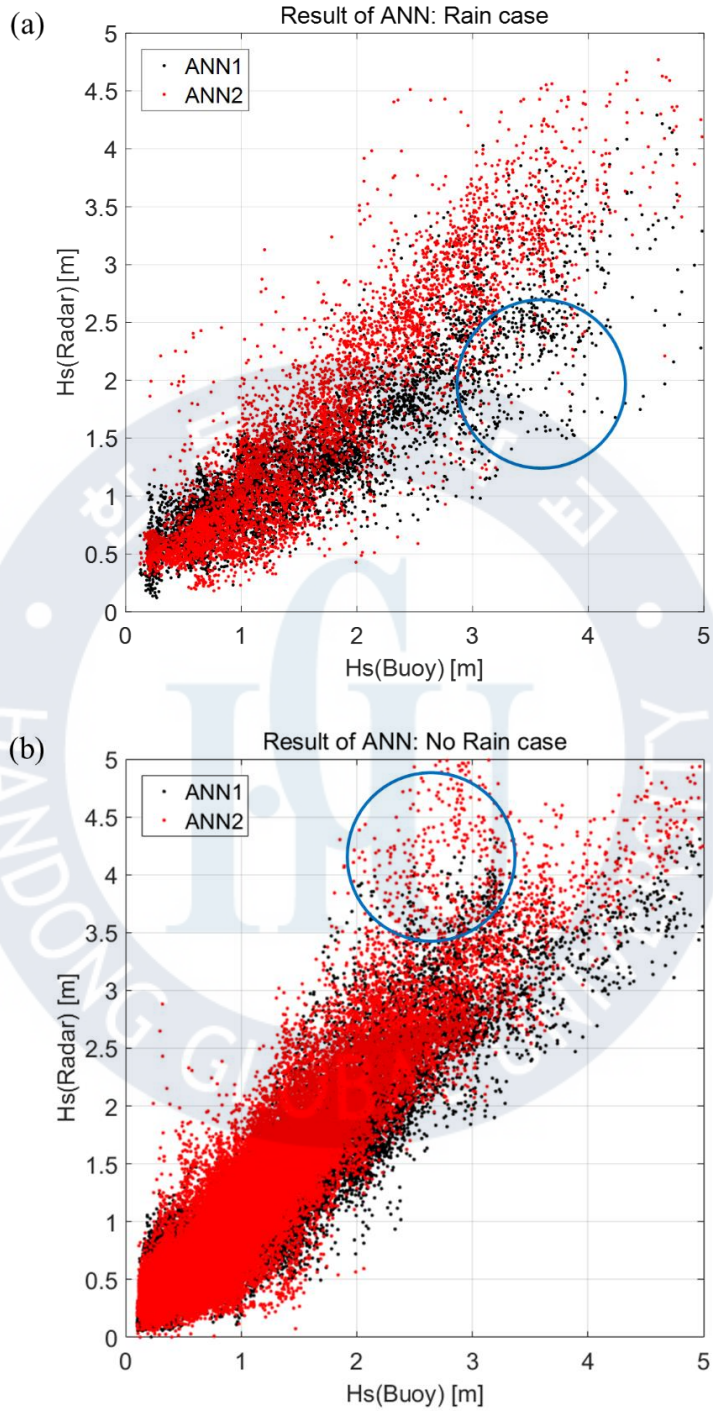

Figure 29. Regressions of estimated Hs and Hs buoy. (a) rain data, (b) no-rain data.

These regressions prove that ANN1 estimates Hs well in normal case, and ANN2 estimates Hs well in rainfall. The main idea of the proposed algorithm of this study is found here. The final Hs is estimated by selecting an ANN model according to its rainfall label and applying the model.

4.2.3 Application of ANN models

According to the observation in 4.2.2, two models are alternatively used along rainfall. Figure 30 briefly shows the flow of model application of a single data. There are pre-trained models, ANN1 and ANN2. If i^{th} time rainfall label is 0(0 means No-rain), the algorithm selects ANN1 and i^{th} time input data is applied to it. Contrary, i^{th} rainfall label is 1(1 means Rain), the algorithm selects ANN2 and i^{th} time input data is applied to ANN2. Then, i^{th} Hs is calculated. Final Hs result is merging all components of time series, Hs_i.

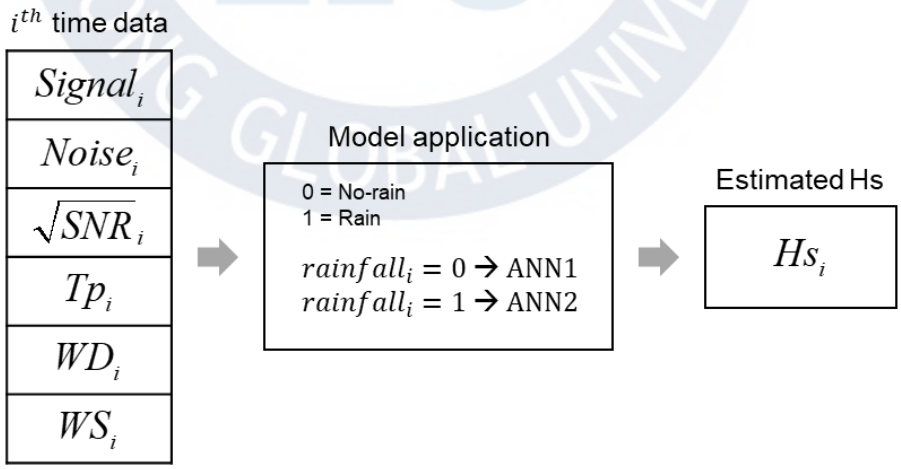

Figure 30. Flow of model application of a single data

4.3 Results and discussion

Estimated Hs

Hs estimation results of the algorithm proposed in this study are shown in Figure 31 as a regression graph together with the buoy Hs. Figure 31 (a) is the result of single ANN method which is used in existing study and the coefficient of determination is 0.81. Figure 31 (b) is the result of multiple ANN which is proposed in this study, and the coefficient of determination is slightly increased to 0.85. Although the number increase is quite small, it is found that the underestimated typhoon season data is retrieved. It is natural that the numerical increase is small because the number of data during rainfall is significantly smaller than that of non-rainfall data.

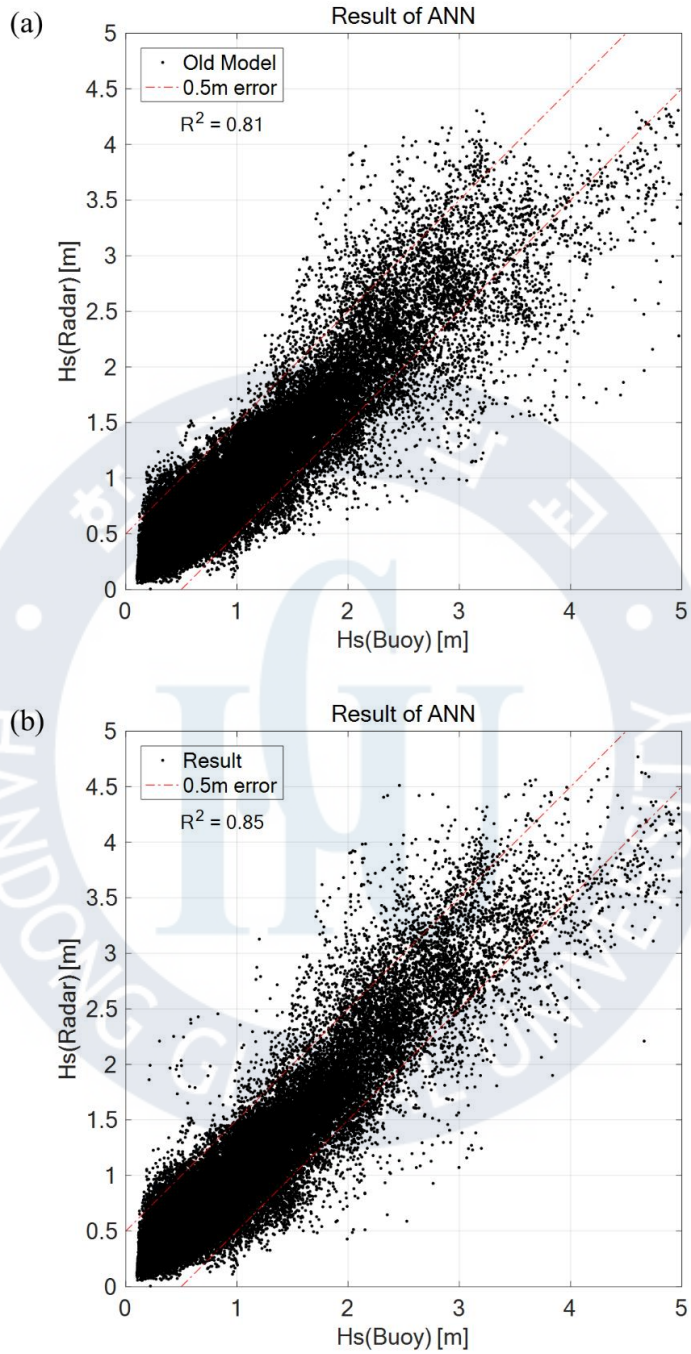

Figure 31. Regression of results (a) single ANN (b) multiple ANN(the proposed algorithm)

5. CONCLUSION

Rainfall was classified from the X-band radar image using CNN. In addition, by applying the results to an ANN model of an X-band radar wave height system, Hs estimation algorithm based on the ANN model which can calculate the real time Hs is proposed.

Using the CNN model, it was possible to classify the rainfall noise of X-band radar images, and the classification accuracy was 93.9%. As a result of checking 6.4% of the misclassified data, most of the errors accounted for the case of misclassification as rainfall data even though it was data of non-rainfall. This is because waves appeared densely in the misclassified radar images. Though the accuracy was improved to a high level by manually adjusting the training dataset, it is considered that the error can be further reduced by increasing the ratio of radar image data in which waves appear well during non-rainfall in the training dataset.

As a result of applying different ANN models for calculating the Hs according to rainfall, the result showed significantly improved Hs during rainfall or typhoon than the existing algorithm that calculates the Hs only with a single model without considering rainfall. As a result of analyzing the correlation between the Hs results of the proposed algorithm and the Hs data of the Gyeongpodae Beach Ocean Observatory, the coefficient of determination slightly increased from 0.81 to 0.85. This is mainly because the improved data are rain data, but the numerical improvement is not large because the proportion of the rain data is small. In particular, it was confirmed that the high-wave data during typhoon and rainfall, which were underestimated, were corrected.

On the other hand, the first thought that comes to mind when using different ANN models is training two models(for example, ANN-a and ANN-b) along the rainfall. In other words,

input variables are separated at the first step of ANN along the rainfall T/F label. Therefore, the trained model ANN-a is only for no-rain data, and ANN-b is only for rain data. This algorithm was tried but there was no significant improvement in the accuracy of calculating Hs.

In closing, the proposed algorithm was selected based on rainfall only, and the Hs was calculated by applying different ANN models. However, in order to calculate the Hs stably even under typhoons or severe weather conditions without rainfall, it would be better to additionally consider information such as whether there is a typhoon forecast or not.

6. REFERENCES

1. Ahn, K., Chun, J., & Cheon, S. H. (2014). New calibration method applicable to significant wave heights obtained by X-band radar. Coastal Engineering Proceedings, (34), 15-15.
2. Alpers, W., & Hasselmann, K. (1982). Spectral signal to clutter and thermal noise properties of ocean wave imaging synthetic aperture radars. International Journal of Remote Sensing, 3(4), 423-446.
3. Behnke, S. (2003). Hierarchical neural networks for image interpretation-Introduction. Hierarchical neural networks for image interpretation, 2766, 1-+.
4. Gomez, R., Helzel, T., Petersen, L., Kniephoff, M., Merz, C.R., Liu, Y. and Weisberg, R.H. (2014). Real-time quality control of current velocity data on individual grid cells in WERA HF radar. Oceans 2014-Taipei, IEEE, 1-7.
5. Gurgel, K.W., Schlick, T., Voulgaris, G., Seemann, J. and Ziemer, F. (2011). HF radar observations in the German Bight: Measurements and quality control. IEEE, 51-56.
6. Hakim, A. L. (2020, April). Rain detection in image using convolutional neural network. In Journal of Physics: Conference Series (Vol. 1528, No. 1, p. 012010). IOP Publishing.
7. Hisaki, Y. (2009). Quality control of surface wave data estimated from low signal-to-noise ratio HF radar Doppler spectra. Journal of atmospheric and oceanic technology, 26(11), 2444-2461.
8. Huang, N. E., Shen, Z., Long, S. R., Wu, M. C., Shih, H. H., Zheng, Q., ... & Liu, H. H. (1998). The empirical mode decomposition and the Hilbert spectrum for nonlinear and non-stationary time series analysis. Proceedings of the Royal Society of London.

Series A: mathematical, physical and engineering sciences, 454(1971), 903-995.

9. Jun, H., Min, Y., Jeong, J. Y., & Do, K. (2020). Measurement and Quality Control of MIROS Wave Radar Data at Dokdo. Journal of Korean Society of Coastal and Ocean Engineers, 32(2), 135-145.
10. LeCun, Y., Boser, B., Denker, J. S., Henderson, D., Howard, R. E., Hubbard, W., & Jackel, L. D. (1989). Backpropagation applied to handwritten zip code recognition. Neural computation, 1(4), 541-551.
11. Liu, X., Huang, W., & Gill, E. W. (2016). Wave height estimation from shipborne X-band nautical radar images. Journal of Sensors, 2016.
12. Liu, X., Huang, W., & Gill, E. W. (2016). Wind direction estimation from rain-contaminated marine radar data using the ensemble empirical mode decomposition method. IEEE Transactions on Geoscience and Remote Sensing, 55(3), 1833-1841.
13. Nieto Borge, J., RodrÍguez, G. R., Hessner, K., & González, P. I. (2004). Inversion of marine radar images for surface wave analysis. Journal of Atmospheric and Oceanic Technology, 21(8), 1291-1300.
14. Nieto-Borge, J. C., Hessner, K., Jarabo-Amores, P., & De La Mata-Moya, D. (2008). Signal-to-noise ratio analysis to estimate ocean wave heights from X-band marine radar image time series. IET Radar, Sonar & Navigation, 2(1), 35-41.
15. Park, J.S., Ahn, K. and Oh, C.Y., (2017). Calibration of Significant Wave Height Obtained by X-band Radar using Artificial Neural Networks, Proceedings of Coastal and Ocean Engineering in Korea, 25, 132-135.
16. Simard, P. Y., Steinkraus, D., & Platt, J. C. (2003, August). Best practices for convolutional neural networks applied to visual document analysis. In Icdar (Vol. 3,

No. 2003).

17. Vicen-Bueno, R., Lido-Muela, C., & Nieto-Borge, J. C. (2012). Estimate of significant wave height from non-coherent marine radar images by multilayer perceptrons. EURASIP Journal on Advances in Signal Processing, 2012(1), 84.

APPENDIX

A. Summary of Hs estimation during the typhoon Maysak(2020/09/03)

Date	CNN Rainfall Classification	ANN Model Application	Reference Hs (m)	Estimated Hs (m)
2020-09-03 0:00	Rain	ANN2	1.76	1.92
2020-09-03 0:10	No-rain	ANN1	1.74	1.35
2020-09-03 0:20	No-rain	ANN1	1.76	1.37
2020-09-03 0:30	No-rain	ANN1	1.77	1.39
2020-09-03 0:40	No-rain	ANN1	1.76	1.45
2020-09-03 0:50	No-rain	ANN1	1.74	1.44
2020-09-03 1:00	No-rain	ANN1	1.72	1.34
2020-09-03 1:10	No-rain	ANN1	1.72	1.44
2020-09-03 1:20	No-rain	ANN1	1.69	1.49
2020-09-03 1:30	No-rain	ANN1	1.70	1.34
2020-09-03 1:40	No-rain	ANN1	1.69	1.28
2020-09-03 1:50	No-rain	ANN1	1.68	1.22
2020-09-03 2:00	No-rain	ANN1	1.66	1.39
2020-09-03 2:10	No-rain	ANN1	1.70	1.48
2020-09-03 2:20	No-rain	ANN1	1.75	1.46
2020-09-03 2:30	No-rain	ANN1	1.74	1.47
2020-09-03 2:40	No-rain	ANN1	1.79	1.28
2020-09-03 2:50	No-rain	ANN1	1.80	1.34
2020-09-03 3:00	No-rain	ANN1	1.82	1.47
2020-09-03 3:10	No-rain	ANN1	1.85	1.45
2020-09-03 3:20	No-rain	ANN1	1.90	1.33
2020-09-03 3:30	Rain	ANN2	1.98	1.66
2020-09-03 3:40	Rain	ANN2	2.05	1.48
2020-09-03 3:50	Rain	ANN2	2.09	1.33
2020-09-03 4:00	Rain	ANN2	2.17	1.95
2020-09-03 4:10	Rain	ANN2	2.24	2.23
2020-09-03 4:20	Rain	ANN2	2.30	3.05
2020-09-03 4:30	Rain	ANN2	2.43	3.26
2020-09-03 4:40	Rain	ANN2	2.52	3.27
2020-09-03 4:50	Rain	ANN2	2.65	3.69
2020-09-03 5:00	Rain	ANN2	2.75	3.69
2020-09-03 5:10	Rain	ANN2	2.86	3.19
2020-09-03 5:20	Rain	ANN2	2.92	3.46
2020-09-03 5:30	Rain	ANN2	3.01	3.45

2020-09-03 5:40	Rain	ANN2	3.19	3.22
2020-09-03 5:50	Rain	ANN2	3.33	3.53
2020-09-03 6:00	Rain	ANN2	3.59	3.51
2020-09-03 6:10	Rain	ANN2	3.85	3.50
2020-09-03 6:20	Rain	ANN2	4.12	3.37
2020-09-03 6:30	Rain	ANN2	4.32	3.63
2020-09-03 6:40	Rain	ANN2	4.48	3.84
2020-09-03 6:50	Rain	ANN2	4.66	4.09
2020-09-03 7:00	Rain	ANN2	4.79	3.59
2020-09-03 7:10	Rain	ANN2	4.81	3.41
2020-09-03 7:20	Rain	ANN2	4.92	3.87
2020-09-03 7:30	Rain	ANN2	4.98	4.10
2020-09-03 7:40	Rain	ANN2	5.05	4.23
2020-09-03 7:50	Rain	ANN2	5.02	4.35
2020-09-03 8:00	No-rain	ANN1	4.99	3.55
2020-09-03 8:10	No-rain	ANN1	4.83	3.67
2020-09-03 8:20	Rain	ANN2	4.74	4.33
2020-09-03 8:30	Rain	ANN2	4.67	4.62
2020-09-03 8:40	Rain	ANN2	4.61	4.77
2020-09-03 8:50	Rain	ANN2	4.47	4.31
2020-09-03 9:00	Rain	ANN2	4.42	4.42
2020-09-03 9:10	Rain	ANN2	4.33	4.59
2020-09-03 9:20	Rain	ANN2	4.19	4.47
2020-09-03 9:30	Rain	ANN2	3.97	4.49
2020-09-03 9:40	Rain	ANN2	3.77	4.42
2020-09-03 9:50	Rain	ANN2	3.65	4.51
2020-09-03 10:00	Rain	ANN2	3.44	4.43
2020-09-03 10:10	Rain	ANN2	3.25	4.32
2020-09-03 10:20	Rain	ANN2	3.09	3.96
2020-09-03 10:30	Rain	ANN2	2.96	4.20
2020-09-03 10:40	Rain	ANN2	2.90	4.32
2020-09-03 10:50	Rain	ANN2	2.76	4.43
2020-09-03 11:00	Rain	ANN2	2.64	4.42
2020-09-03 11:10	Rain	ANN2	2.46	4.51
2020-09-03 11:20	Rain	ANN2	2.35	4.42
2020-09-03 11:30	No-rain	ANN1	2.36	3.18
2020-09-03 11:40	Rain	ANN2	2.32	4.41
2020-09-03 11:50	No-rain	ANN1	2.29	2.93
2020-09-03 12:00	Rain	ANN2	2.38	3.98

2020-09-03 12:10	No-rain	ANN1	2.41	3.06
2020-09-03 12:20	Rain	ANN2	2.33	3.77
2020-09-03 12:30	No-rain	ANN1	2.27	2.89
2020-09-03 12:40	No-rain	ANN1	2.14	2.82
2020-09-03 12:50	Rain	ANN2	2.03	3.35
2020-09-03 13:00	No-rain	ANN1	1.91	2.51
2020-09-03 13:10	No-rain	ANN1	1.84	2.61
2020-09-03 13:20	No-rain	ANN1	1.79	2.47
2020-09-03 13:30	Rain	ANN2	1.78	3.24
2020-09-03 13:40	No-rain	ANN1	1.74	2.44
2020-09-03 13:50	Rain	ANN2	1.71	2.74
2020-09-03 14:00	No-rain	ANN1	1.72	2.57
2020-09-03 14:10	No-rain	ANN1	1.71	2.41
2020-09-03 14:20	No-rain	ANN1	1.68	2.46
2020-09-03 14:30	No-rain	ANN1	1.71	2.58
2020-09-03 14:40	Rain	ANN2	1.73	2.67
2020-09-03 14:50	No-rain	ANN1	1.70	2.32
2020-09-03 15:00	No-rain	ANN1	1.69	2.33
2020-09-03 15:10	No-rain	ANN1	1.65	2.19
2020-09-03 15:20	No-rain	ANN1	1.69	2.27
2020-09-03 15:30	No-rain	ANN1	1.63	2.27
2020-09-03 15:40	No-rain	ANN1	1.61	2.42
2020-09-03 15:50	No-rain	ANN1	1.66	2.09
2020-09-03 16:00	No-rain	ANN1	1.69	2.25
2020-09-03 16:10	No-rain	ANN1	1.62	1.90
2020-09-03 16:20	No-rain	ANN1	1.56	1.73
2020-09-03 16:30	No-rain	ANN1	1.52	1.79
2020-09-03 16:40	No-rain	ANN1	1.48	1.53
2020-09-03 16:50	No-rain	ANN1	1.40	1.62
2020-09-03 17:00	No-rain	ANN1	1.37	1.56
2020-09-03 17:10	No-rain	ANN1	1.39	1.38
2020-09-03 17:20	No-rain	ANN1	1.39	1.41
2020-09-03 17:30	No-rain	ANN1	1.42	1.16
2020-09-03 17:40	No-rain	ANN1	1.38	1.15
2020-09-03 17:50	No-rain	ANN1	1.42	1.10
2020-09-03 18:00	No-rain	ANN1	1.39	1.09
2020-09-03 18:10	No-rain	ANN1	1.42	0.88
2020-09-03 18:20	No-rain	ANN1	1.41	1.14
2020-09-03 18:30	No-rain	ANN1	1.41	1.11

2020-09-03 18:40	No-rain	ANN1	1.37	1.16
2020-09-03 18:50	No-rain	ANN1	1.36	1.14
2020-09-03 19:00	No-rain	ANN1	1.30	1.03
2020-09-03 19:10	No-rain	ANN1	1.29	1.10
2020-09-03 19:20	No-rain	ANN1	1.28	0.89
2020-09-03 19:30	No-rain	ANN1	1.29	0.95
2020-09-03 19:40	No-rain	ANN1	1.30	0.98
2020-09-03 19:50	No-rain	ANN1	1.35	0.81
2020-09-03 20:00	No-rain	ANN1	1.38	0.88
2020-09-03 20:10	No-rain	ANN1	1.36	0.86
2020-09-03 20:20	No-rain	ANN1	1.39	0.85
2020-09-03 20:30	No-rain	ANN1	1.40	0.77
2020-09-03 20:40	No-rain	ANN1	1.39	0.89
2020-09-03 20:50	No-rain	ANN1	1.37	0.88
2020-09-03 21:00	No-rain	ANN1	1.42	0.90
2020-09-03 21:10	No-rain	ANN1	1.44	0.74
2020-09-03 21:20	No-rain	ANN1	1.49	0.78
2020-09-03 21:30	No-rain	ANN1	1.50	0.80
2020-09-03 21:40	No-rain	ANN1	1.57	0.74
2020-09-03 21:50	No-rain	ANN1	1.64	0.90
2020-09-03 22:00	No-rain	ANN1	1.62	0.69
2020-09-03 22:10	No-rain	ANN1	1.67	0.67
2020-09-03 22:20	No-rain	ANN1	1.67	0.66
2020-09-03 22:30	No-rain	ANN1	1.74	0.60
2020-09-03 22:40	No-rain	ANN1	1.69	0.50
2020-09-03 22:50	No-rain	ANN1	1.66	0.58
2020-09-03 23:00	No-rain	ANN1	1.60	0.50
2020-09-03 23:10	No-rain	ANN1	1.58	0.63
2020-09-03 23:20	No-rain	ANN1	1.56	0.53
2020-09-03 23:30	No-rain	ANN1	1.52	0.60
2020-09-03 23:40	No-rain	ANN1	1.51	0.65
2020-09-03 23:50	No-rain	ANN1	1.55	0.63

B. Summary of Hs estimation during the typhoon Haishen(2020/09/07)

Date	CNN Rainfall Classification	ANN Model Application	Reference Hs (m)	Estimated Hs (m)
2020-09-07 0:00	Rain	ANN2	0.99	0.45
2020-09-07 0:10	Rain	ANN2	1.03	0.44
2020-09-07 0:20	Rain	ANN2	1.11	0.33
2020-09-07 0:30	Rain	ANN2	1.14	0.46
2020-09-07 0:40	Rain	ANN2	1.19	0.49
2020-09-07 0:50	Rain	ANN2	1.22	0.52
2020-09-07 1:00	Rain	ANN2	1.25	0.57
2020-09-07 1:10	Rain	ANN2	1.28	0.69
2020-09-07 1:20	No-rain	ANN1	1.29	0.80
2020-09-07 1:30	No-rain	ANN1	1.32	0.94
2020-09-07 1:40	No-rain	ANN1	1.40	0.83
2020-09-07 1:50	No-rain	ANN1	1.45	0.81
2020-09-07 2:00	No-rain	ANN1	1.43	0.79
2020-09-07 2:10	No-rain	ANN1	1.49	0.78
2020-09-07 2:20	Rain	ANN2	1.55	0.77
2020-09-07 2:30	No-rain	ANN1	1.59	0.71
2020-09-07 2:40	No-rain	ANN1	1.59	0.79
2020-09-07 2:50	Rain	ANN2	1.67	0.55
2020-09-07 3:00	Rain	ANN2	1.72	0.63
2020-09-07 3:10	Rain	ANN2	1.76	0.88
2020-09-07 3:20	No-rain	ANN1	1.78	0.77
2020-09-07 3:30	No-rain	ANN1	1.81	0.82
2020-09-07 3:40	Rain	ANN2	1.83	0.94
2020-09-07 3:50	No-rain	ANN1	1.84	0.93
2020-09-07 4:00	Rain	ANN2	1.89	0.86
2020-09-07 4:10	No-rain	ANN1	1.99	1.05
2020-09-07 4:20	Rain	ANN2	2.06	1.31
2020-09-07 4:30	Rain	ANN2	2.20	1.61
2020-09-07 4:40	Rain	ANN2	2.31	1.44
2020-09-07 4:50	Rain	ANN2	2.44	1.34
2020-09-07 5:00	Rain	ANN2	2.45	1.62
2020-09-07 5:10	Rain	ANN2	2.47	1.63
2020-09-07 5:20	Rain	ANN2	2.57	1.20
2020-09-07 5:30	Rain	ANN2	2.61	1.07
2020-09-07 5:40	Rain	ANN2	2.67	1.29
2020-09-07 5:50	Rain	ANN2	2.73	1.83

2020-09-07 6:00	Rain	ANN2	2.82	1.50
2020-09-07 6:10	Rain	ANN2	2.89	2.07
2020-09-07 6:20	Rain	ANN2	2.90	1.95
2020-09-07 6:30	Rain	ANN2	2.90	1.69
2020-09-07 6:40	Rain	ANN2	2.87	1.81
2020-09-07 6:50	Rain	ANN2	2.83	2.37
2020-09-07 7:00	Rain	ANN2	2.86	2.11
2020-09-07 7:10	Rain	ANN2	2.90	1.46
2020-09-07 7:20	Rain	ANN2	2.99	1.57
2020-09-07 7:30	Rain	ANN2	3.11	1.27
2020-09-07 7:40	Rain	ANN2	3.14	1.80
2020-09-07 7:50	Rain	ANN2	3.20	1.24
2020-09-07 8:00	Rain	ANN2	3.15	1.38
2020-09-07 8:10	Rain	ANN2	3.12	1.23
2020-09-07 8:20	Rain	ANN2	3.08	1.63
2020-09-07 8:30	Rain	ANN2	3.07	2.15
2020-09-07 8:40	Rain	ANN2	3.02	2.40
2020-09-07 8:50	Rain	ANN2	3.00	2.03
2020-09-07 9:00	Rain	ANN2	2.98	2.53
2020-09-07 9:10	Rain	ANN2	3.00	2.94
2020-09-07 9:20	Rain	ANN2	3.01	3.24
2020-09-07 9:30	Rain	ANN2	3.03	3.67
2020-09-07 9:40	Rain	ANN2	3.13	3.67
2020-09-07 9:50	Rain	ANN2	3.17	3.61
2020-09-07 10:00	Rain	ANN2	3.21	4.07
2020-09-07 10:10	Rain	ANN2	3.20	3.78
2020-09-07 10:20	Rain	ANN2	3.22	3.86
2020-09-07 10:30	Rain	ANN2	3.23	3.90
2020-09-07 10:40	Rain	ANN2	3.23	4.23
2020-09-07 10:50	Rain	ANN2	3.31	3.89
2020-09-07 11:00	Rain	ANN2	3.40	3.92
2020-09-07 11:10	Rain	ANN2	3.44	4.05
2020-09-07 11:20	Rain	ANN2	3.50	3.92
2020-09-07 11:30	Rain	ANN2	3.63	3.97
2020-09-07 11:40	Rain	ANN2	3.69	4.19
2020-09-07 11:50	Rain	ANN2	3.77	4.06
2020-09-07 12:00	Rain	ANN2	3.85	3.64
2020-09-07 12:10	Rain	ANN2	3.97	3.42
2020-09-07 12:20	Rain	ANN2	4.08	3.69

2020-09-07 12:30	Rain	ANN2	4.23	3.46
2020-09-07 12:40	Rain	ANN2	4.45	3.51
2020-09-07 12:50	Rain	ANN2	4.74	4.16
2020-09-07 13:00	Rain	ANN2	4.97	4.25
2020-09-07 13:10	No-rain	ANN1	5.15	3.02
2020-09-07 13:20	No-rain	ANN1	5.24	3.34
2020-09-07 13:30	No-rain	ANN1	5.39	3.56
2020-09-07 13:40	No-rain	ANN1	5.48	3.55
2020-09-07 13:50	No-rain	ANN1	5.47	3.45
2020-09-07 14:00	No-rain	ANN1	5.44	3.57
2020-09-07 14:10	No-rain	ANN1	5.32	3.52
2020-09-07 14:20	No-rain	ANN1	5.27	3.65
2020-09-07 14:30	No-rain	ANN1	5.18	3.49
2020-09-07 14:40	No-rain	ANN1	5.13	3.51
2020-09-07 14:50	No-rain	ANN1	5.03	3.64
2020-09-07 15:00	No-rain	ANN1	4.96	3.44
2020-09-07 15:10	No-rain	ANN1	4.84	3.56
2020-09-07 15:20	No-rain	ANN1	4.75	3.64
2020-09-07 15:30	No-rain	ANN1	4.61	3.59
2020-09-07 15:40	No-rain	ANN1	4.41	3.65
2020-09-07 15:50	No-rain	ANN1	4.34	3.63
2020-09-07 16:00	No-rain	ANN1	4.22	3.63
2020-09-07 16:10	No-rain	ANN1	4.02	3.55
2020-09-07 16:20	No-rain	ANN1	3.91	3.52
2020-09-07 16:30	No-rain	ANN1	3.78	3.54
2020-09-07 16:40	No-rain	ANN1	3.78	3.46
2020-09-07 16:50	No-rain	ANN1	3.72	3.41
2020-09-07 17:00	No-rain	ANN1	3.77	3.44
2020-09-07 17:10	No-rain	ANN1	3.76	3.42
2020-09-07 17:20	No-rain	ANN1	3.72	3.55
2020-09-07 17:30	No-rain	ANN1	3.65	3.38
2020-09-07 17:40	No-rain	ANN1	3.60	3.37
2020-09-07 17:50	No-rain	ANN1	3.49	3.34
2020-09-07 18:00	No-rain	ANN1	3.41	3.31
2020-09-07 18:10	No-rain	ANN1	3.36	3.28
2020-09-07 18:20	No-rain	ANN1	3.26	3.29
2020-09-07 18:30	No-rain	ANN1	3.25	3.29
2020-09-07 18:40	No-rain	ANN1	3.25	3.10
2020-09-07 18:50	No-rain	ANN1	3.19	3.28

2020-09-07 19:00	No-rain	ANN1	3.13	2.88
2020-09-07 19:10	No-rain	ANN1	3.10	2.84
2020-09-07 19:20	No-rain	ANN1	3.04	2.73
2020-09-07 19:30	No-rain	ANN1	2.91	2.15
2020-09-07 19:40	No-rain	ANN1	2.76	2.23
2020-09-07 19:50	No-rain	ANN1	2.73	2.11
2020-09-07 20:00	No-rain	ANN1	2.68	1.83
2020-09-07 20:10	No-rain	ANN1	2.65	2.05
2020-09-07 20:20	No-rain	ANN1	2.59	1.76
2020-09-07 20:30	No-rain	ANN1	2.61	1.64
2020-09-07 20:40	No-rain	ANN1	2.62	1.95
2020-09-07 20:50	No-rain	ANN1	2.61	1.74
2020-09-07 21:00	No-rain	ANN1	2.50	1.54
2020-09-07 21:10	No-rain	ANN1	2.41	1.80
2020-09-07 21:20	No-rain	ANN1	2.38	1.99
2020-09-07 21:30	No-rain	ANN1	2.35	1.93
2020-09-07 21:40	No-rain	ANN1	2.30	1.79
2020-09-07 21:50	No-rain	ANN1	2.27	1.48
2020-09-07 22:00	No-rain	ANN1	2.27	1.68
2020-09-07 22:10	No-rain	ANN1	2.21	1.72
2020-09-07 22:20	No-rain	ANN1	2.19	1.69
2020-09-07 22:30	No-rain	ANN1	2.21	1.81
2020-09-07 22:40	No-rain	ANN1	2.20	1.65
2020-09-07 22:50	No-rain	ANN1	2.23	1.43
2020-09-07 23:00	No-rain	ANN1	2.21	1.66
2020-09-07 23:10	No-rain	ANN1	2.19	1.71
2020-09-07 23:20	No-rain	ANN1	2.19	1.47
2020-09-07 23:30	No-rain	ANN1	2.13	1.42
2020-09-07 23:40	No-rain	ANN1	2.09	1.29
2020-09-07 23:50	No-rain	ANN1	2.06	1.25